Running on empty: Mitochondria without mtDNA exhibit differential motility and connectivity

Joanna M. Chustecki[1], Alora Q. Schneider[1], Madeleine H. Faber[1], Alan C. Christensen[1*]

1 School of Biological Sciences, University of Nebraska-Lincoln, USA.

*Corresponding author email: achristensen2@unl.edu

Abstract

Plant mitochondria are in continuous motion. While providing ATP to other cellular processes, they also constantly consume ATP to move rapidly within the cell. This movement is in part related to taking up, converting and delivering metabolites and energy to and from different parts of the cell. Plant mitochondria have varying amounts of DNA even within a single cell, from none to the full mitochondrial genome. Because mitochondrial dynamics are altered in a mutant with disrupted DNA maintenance, we hypothesised that exchanging DNA templates for repair is one of the functions of their movement and interactions. Here, we stain mitochondrial DNA while tracking mitochondrial position to investigate differences in the behaviour of mitochondria with and without DNA. We have also developed a fluorescent mitochondrial DNA binding protein that will enable future understanding of mitochondrial dynamics, genome maintenance and replication. We demonstrated that mitochondria without mtDNA have altered physical behaviour and have a lower immediate connectivity to the rest of the population, further supporting a link between the physical and genetic dynamics of these complex organelles.

Introduction

Mitochondria are highly dynamic, bioenergetic organelles. In most plant cells, mitochondrial populations exist as individual organelles, moving about the cell interacting with each other and other organelles, while remaining evenly spread across the cell (Chustecki *et al.*, 2021). This movement is mostly facilitated by myosin motors upon actin filaments (Avisar et al., 2009; Romagnoli et al., 2007). This dynamic

behaviour may be important for taking up, converting, and delivering metabolites and energy to different parts of the cell, and for exchanging mitochondrial contents. In contrast to other kingdoms, not all mitochondria in plant cells carry mitochondrial DNA (mtDNA) (Arimura *et al.*, 2004; Preuten *et al.*, 2010; Gualberto *et al.*, 2014; Kozik *et al.*, 2019). Some individuals carry the full complement of genes, or a subgenomic molecule, while others carry none. Exchange of mtDNA between mitochondria in plant cells has been demonstrated on the level of single organelles (Sheahan *et al.* 2005; Arimura, 2018), and this exchange may allow each individual to access the full complement of genes and gene products over time (Giannakis *et al*., 2022). Plants also exhibit high levels of mtDNA recombination and varied physical forms of nucleoids, including linear and branched (Kozik et al., 2019). Mitochondrial interactions therefore offer another level of control for DNA maintenance, repair and recombination (Johnston, 2019). This link between the *physical* and *genetic* dynamics of plant mitochondria is not yet well-understood.

Colocalisation, fission and fusion events as well as ‘kiss-and-run’ membrane sharing dynamics have functional implications for plant mitochondria (Bauwe et al., 2010; Christensen, 2014; Hagemann et al., 2016; Midorikawa et al., 2022; Mueller & Reski, 2015; White et al., 2020). This interacting population has been demonstrated to homogenise mitochondrial contents, explicitly seen in onion epidermal cells over a few hours (Arimura et al., 2004). Therefore, the idea of a ‘discontinuous whole’’, has emerged (Logan, 2006). While some developmental stages and cell types have reticulated mitochondrial structure, (such as the shoot apical meristem (ref), or germinating embryos (ref)), individual mitochondria in most plant cells *transiently* and *continuously* share their contents. Being interconnected without being physically connected provides a level of physical control over content sharing (Johnston, 2019).

Disruption of the organellar DNA repair gene MSH1 imposed a genetic challenge to the mitochondrial genome, leading to increased colocalisation times and network connectivity (Chustecki *et al.*, 2021). This was hypothesised as a response to increased sharing due to individual mitochondria needing to access undamaged mtDNA templates for double-strand break repair (Chustecki *et al.*, 2022; Rodriguez *et al.*, 2022). This

leads directly to the hypothesis that the mitochondrial genome is an important influence on mitochondrial dynamics and network behavior.

To test this hypothesis, we developed a system to assess whether the dynamics of mitochondria with and without DNA are different. We used a combination of *Arabidopsis* single-cell confocal microscopy, tracking of dynamic movement, and network analysis to characterise the behaviour and correlate it to the presence or absence of DNA. We also introduce a new mitochondrial-DNA binding photoconvertible fluorescent protein to *Arabidopsis*, providing a new tool to quantify, track and reveal mtDNA dynamics in live cells, eliminating the need for exogenous stains. We present data showing a link between mitochondrial DNA, mitochondrial dynamics and social behaviour.

Results

Plant cells show a persistent population of mitochondria without mtDNA

It has previously been shown that individual mitochondria in plant cells do not carry the full gene complement. Some do carry the full complement, while some carry a subgenomic molecule(s) with a few genes, and some have no mtDNA at all (Arimura et al., 2004; Gualberto et al., 2014; Kozik et al., 2019; Logan, 2006; Preuten et al., 2010; Takanashi et al., 2006). To quantify the proportion of mitochondria with and without mtDNA in *whole* single cells, across two cell types, we fixed 5-day old *Arabidopsis* seedlings encoding mitochondrially-targeted mCherry (Kindly provided by Prof. Markus Schwarzländer (pBin atp-mCherry, (Candat et al., 2014))). These were stained with SYBR green, an intercalating dye specific for double stranded DNA (dsDNA), with a low affinity for RNA (Zipper *et al.*, 2004; Arya *et al.*, 2005; Dragan *et al.*, 2012). Cells (8 hypocotyl cells and 11 leaf epidermal cells) were imaged using a confocal laser scanning microscope and segmented using IMARIS (see methods). The SYBR stain gives a signal for all dsDNA in the cell, including the nucleus and chloroplast, alongside the mitochondrial DNA signal of interest (Figure 1A.i,ii). Some organelles contain no mtDNA, while others have a range of weaker to stronger SYBR signals, all able to be

detected by the segmentation thresholds (Figure 1B). Only the SYBR signal that sits directly within mitochondrial volumes was quantified, avoiding other organellar DNA signals. This method revealed a persistent but varied proportion of mitochondria that do not carry genomic material, (Figure 1C, see methods), confirming previous results.

Both the proportion and absolute number of mitochondria not carrying genomic material vary both across and within cell types. As controls for the segmentation process, a Col-0 (wild-type, with no stable fluorescent marker) hypocotyl cell treated with SYBR, and a mito-mCherry hypocotyl cell with no SYBR stain were also segmented, giving similar intensity and mitochondrial volumes, respectively (Figure S1). We also see a correlation between cell area and mitochondrial number, explaining the variation in total mitochondrial number across cells (Figure S2). This staining and segmentation offers a cell-by-cell quantification of mtDNA presence/absence, supporting previous observations of mitochondria without genomic material.

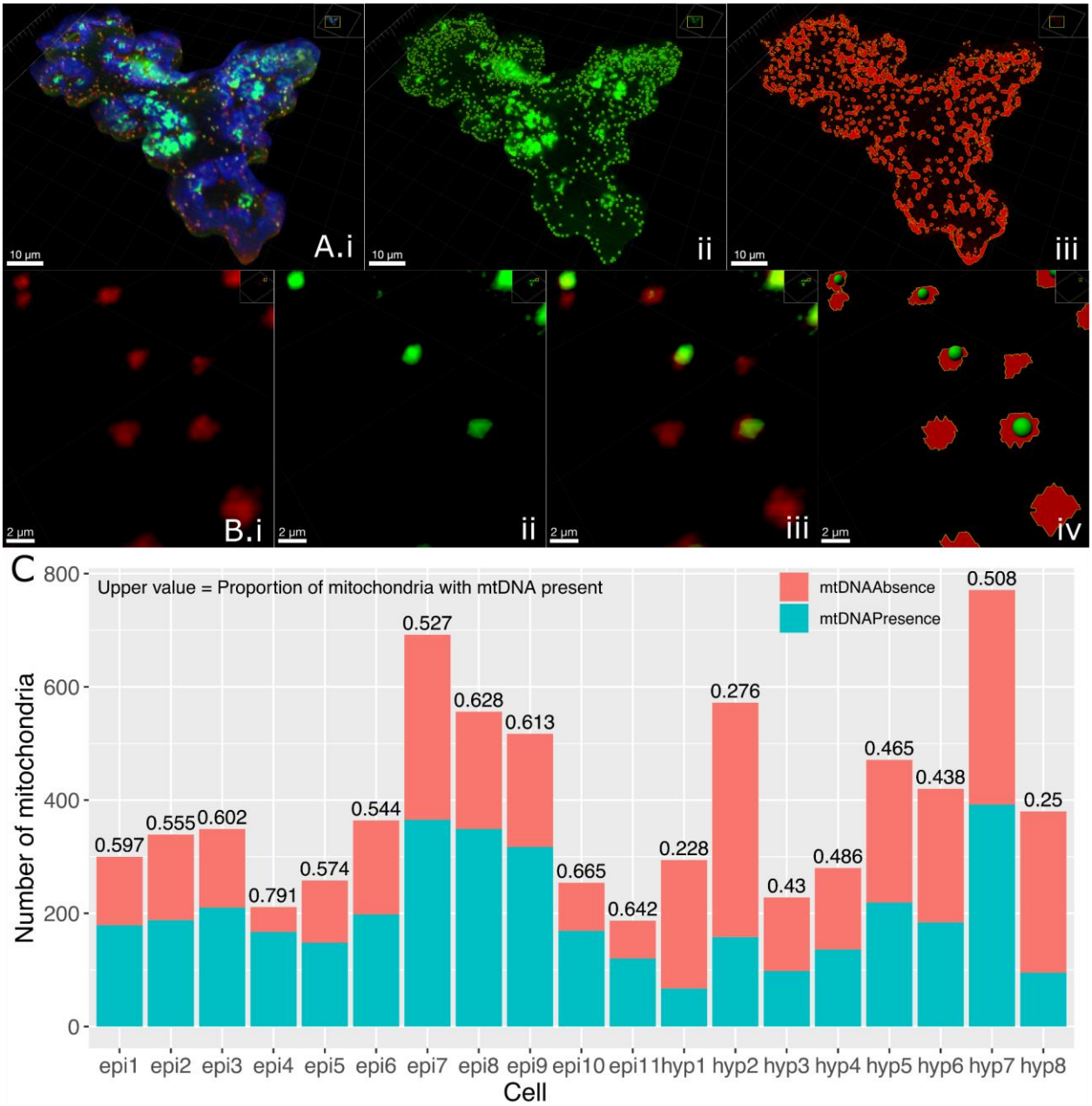

Figure 1: Quantification of mitochondria with and without mtDNA presence in fixed single plant cells A) (i) A single, fixed, leaf epidermal cell with mito-mCherry marker (red), SYBR green staining ds-DNA (green), and chloroplast autofluorescence (blue). (ii) SYBR channel with segmented puncta of ds-DNA signal, (ii) mito-mCherry channel with thresholded 3D rendering of mitochondria. All (A) are Z-stacks of 40 x 0.3µm slices, whole cell rendered in IMARIS.

B) Magnified portion of cell shown in (A), with (i) the mito-Cherry signal, (ii) the SYBR signal, (iii) both mito-mCherry signal and SYBR signal, (iv) thresholded 3D rendering of both channels segmented using the IMARIS cell model.
C) Number of mitochondria with or without mtDNA following IMARIS segmentation. Height of bars is total number of mitochondria, mtDNA absent number is in coral (upper part of bar), mtDNA present number is in blue, (lower part of bar). Value printed above bars is the proportional value of mitochondria with mtDNA present. 'epi'= leaf epidermal cell, 'hyp' = hypocotyl cell.

<u>Defining mtDNA presence or absence in time-lapses of mitochondrial dynamics</u>

To investigate the hypothesised link between the physical and genetic dynamics of plant mitochondria, we characterised the movement of individual organelles with and without mtDNA. Laser scanning confocal time lapses of 5-day old mito-mCherry hypocotyl cells stained with the dsDNA marker SYBR green were captured over ~4 mins (Figure 2A, Video 1). Hypocotyl cells were chosen as they have been demonstrated to provide a quasi-2D field of view of the mitochondrial population, and the cellular geography allows clear tracking of individual organelles (Chustecki *et al.*, 2021).

Tracking was performed using Trackmate (Tinevez *et al.*, 2017), upon the mito-mCherry channel of the captured videos, followed by manual verification. The SYBR green channel was then used to define mtDNA presence or absence, and did not influence the tracking. Trackmate quantification results can be viewed as a trajectory map over time (Figure 2B).

Two approaches were tested to quantify SYBR signal in the GFP channel. Firstly, Trackmate quantifies the signal in each dot encircling the tracked mitochondrion. From this, the contrast statistic was used to define presence or absence of mtDNA (Tinevez et al., 2017). Contrast is calculated as the Intensity (A.U) of pixels inside the spot radius (r) compared to outside as defined by $2r$ by $(I_{in}-I_{out})/(I_{in}+I_{out})$ (based on (Michelson, 1995)). This is a good indicator of SYBR signal for punctate mitochondria (Figure S3A). However due to the intensity considered for I_{out}, two distinct SYBR signals that sit within $2r$ of each other may interfere with the contrast calculation, leading to only one being

accounted for. Therefore we also use a second definition of absence/presence, inspired by the flexible parameter Prominence within mtFociCounter (Rey et al., 2023), implementing the Find Maxima function in ImageJ (Wagner, 2016), which scans each pixel intensity value, and in analogy to geographic topography, finds the maxima in relation to those surrounding it. Find Maxima distinguishes two proximal SYBR signals more effectively than the previously defined contrast value (Figure 2C, S3A), and was carried forward as the detection method used.

The next challenge was describing the presence/absence of mtDNA across time points of individual trajectories. The complexity and speed of mitochondrial dynamics in live plant cells poses a challenge for all tracking software. Correlating SYBR signal at each time point for each mitochondrion, it was observed that organelles with no SYBR signal may occasionally have a single frame that crosses the threshold for signal (here Maxima, (Figure S3D)). This could be due to an unspecific SYBR signal or crossing paths with a mitochondrion with a strong SYBR signal. It could also be that those trajectories with SYBR signal may have a few frames where the signal is below the threshold (either defined by Contrast or Maxima). We therefore implemented and evaluated three definitions for mtDNA ‘presence’ for trajectories - based on how many frames a mitochondrial trajectory needs to have a SYBR signal above a threshold for it to be categorised as having mtDNA. The first definition, which we will refer to as *lenient, is that* only one frame in the entire trajectory needs to be above a threshold value to define that mitochondrion as having mtDNA. The next is *tolerant*, where at least two adjacent frames must be above a threshold. The last definition is *strict*, where at least three adjacent frames must be above a threshold. This last definition necessarily excludes all trajectories that are only two frames long. Also, it should be noted, these are definitions of mtDNA presence, aiming to find a balance between accurately defining presence, while not allowing a leaky absent definition to be populated by trajectories with signal.

The most lenient definition appears to allow too many false positives, while the strictest results in a high loss of data (Figure 2D). Therefore, we settled upon the tolerant definition moving forward. Paired with the Find Maxima SYBR detection method, we are limiting false detection, while allowing flexibility to work around any mis-

tracking through the software. This allows us to confidently define and detect mtDNA per trajectory for the subsequent physical statistical analysis.

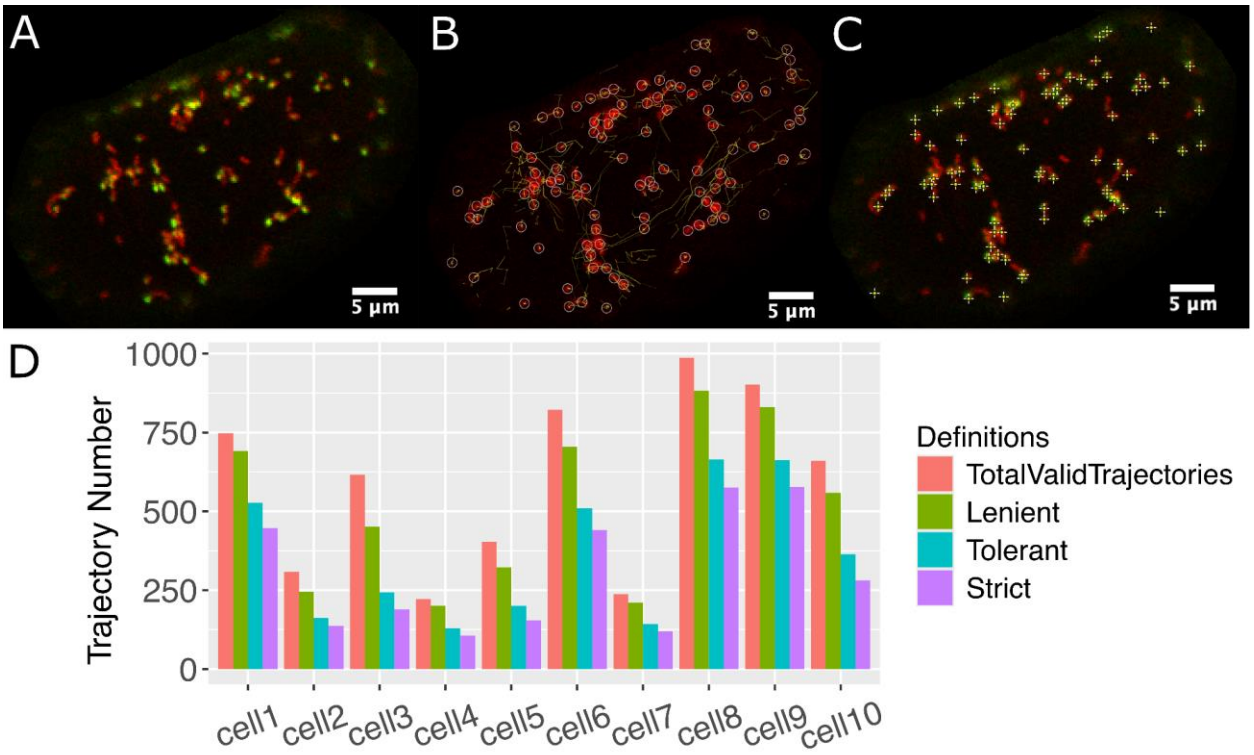

Figure 2: Detecting and defining mtDNA presence. A-C; Single *Arabidopsis* hypocotyl cell with mito-mCherry marker, stained with SYBR green, still frame from time lapse. B) Detected mitochondria (red) using Trackmate (white circles, diameter 1.1µm) with trajectories of mitochondrial motion (yellow), limited to ten frames for clarity. C) SYBR green signal puncta highlighted (white crosses) upon points of intensity classified by Find Maxima function. D) Quantification of trajectory number over total, alongside three definitions of mtDNA presence, in order of strictness, across 10 single hypocotyl cells.

<u>Mitochondria without mtDNA demonstrate altered physical dynamics</u>

Using positional data of mitochondrial movement, and the previously described *tolerant* definition of mtDNA presence/absence, physical statistics of individual mitochondria with and without mtDNA were compared (see methods). First, mean speed was calculated per trajectory, and no difference was observed between mitochondria with and without

mtDNA, across ten hypocotyl cells (Figure 3A). When comparing the mean area travelled per trajectory, a significantly smaller area is travelled by mitochondria without mtDNA (Figure 3B), despite no overall difference in speed. Area travelled is necessarily dependent both on speed, direction, and in this case, trajectory length. We see a difference in trajectory length between those with and without mtDNA, where mitochondria without mtDNA have shorter trajectory duration (Figure S4A). To investigate this further, we implemented the *most extreme* possible definitions of mtDNA presence and absence: every single time point in a trajectory must pass the Maxima threshold to count as that mitochondrion having mtDNA, and every single time point in those without mtDNA must be below the Maxima threshold. Trajectories where not every time point was either with or without DNA were discarded. In this case, we see similar trajectory lengths, but still a smaller area travelled by mitochondria without mtDNA, confirming that this relationship holds without artefact from presence/absence definitions (Figure S4B,C).

Returning to our *tolerant* definition of mtDNA presence/absence, when comparing intermitochondrial positioning, we see differences between mitochondria with and without mtDNA. Intermitochondrial distance is the minimum Euclidean distance between each mitochondrion in each trajectory, averaged per frame. Mitochondria without mtDNA show an increased intermitochondrial distance, meaning they are on average further away from every other mitochondrion in the system than those with mtDNA (Figure 3C). Following this, to test the propensity for sharing between mitochondria, colocalisation time was calculated as the number of frames mitochondria had been within 1.6µm distance of each other (as in (Chustecki *et al.*, 2021)). There is a shorter colocalization time between those without mtDNA and any other mitochondrion it comes into close contact with, than those that do have mtDNA (Figure 3D). Thus, a difference in movement between those with mtDNA and without mtDNA is observed, across whole populations of mitochondria in single cells.

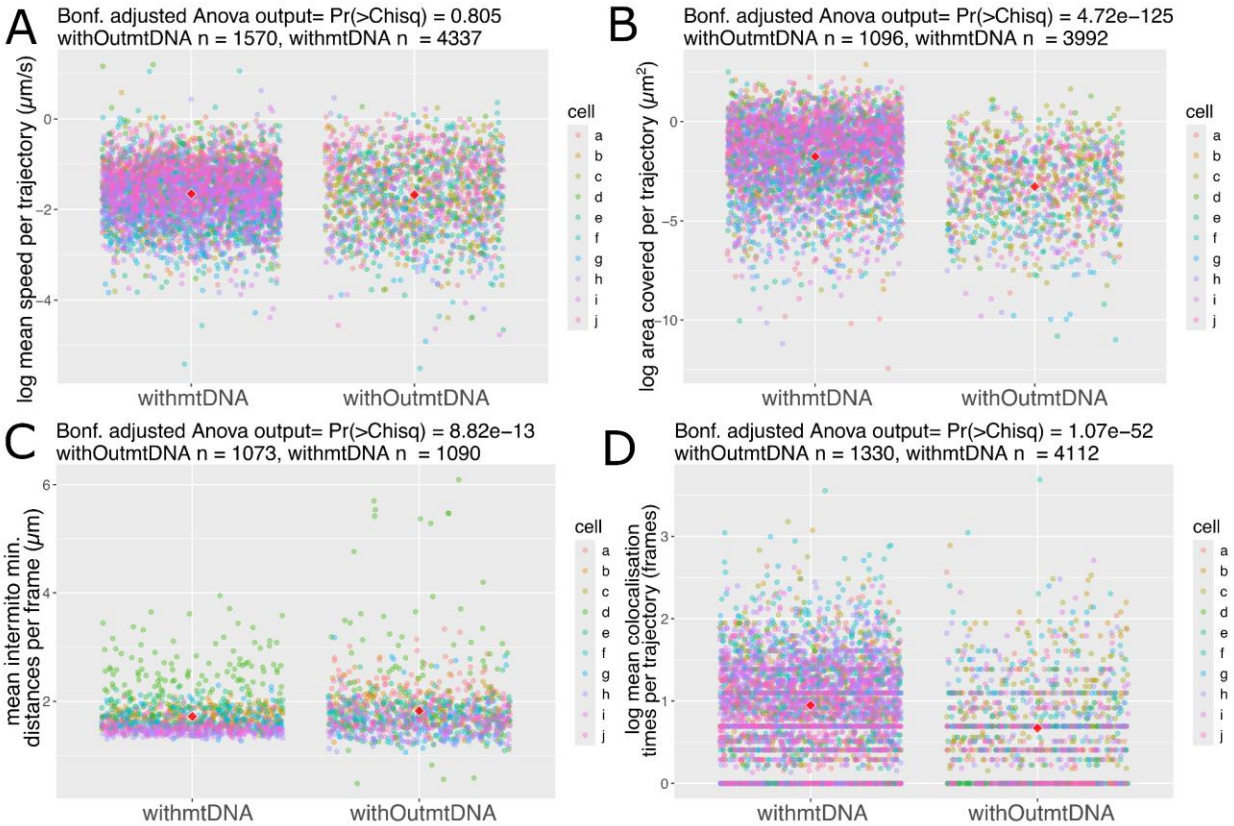

Figure 3: Physical statistics of mitochondrial motion compared between mitochondria defined as with/without mtDNA, across n= 10 hypocotyl cells over 240 seconds of frame time A) Mean speed calculated per trajectory B) Convex hull, the area inside a polygon of the furthest points in a trajectory C) Minimum Euclidean distance between a single mitochondrion and all others, averaged per frame for with/without mtDNA. D) Number of frames individual mitochondria are colocalised to any other. P-values are the outcome of a blocking factor Anova (cells as block), adjusted across all statistics tested using the Bonferroni method. All plots use the *tolerant* definition of mtDNA presence/absence. Red diamonds represent the mean of all points.

<u>Mitochondria without mtDNA are less well connected to the rest of the population.</u>

To study mitochondrial connectivity across whole populations of individual organelles, a novel method borrowing from graph theory, analogous to social networks, has been

developed (Chustecki *et al.*, 2021). Defining individual mitochondria as nodes (here represented as circles), and close connectivity (within 1.6µm distance) as a connecting edge (represented as sticks), we can successfully build historical networks describing and quantifying the interactions of individual organelles over time lapse videos of motion in single cells. Onto this, we project for the first time, functional data - the presence or absence of mtDNA. We define each trajectory as with/without mtDNA and build an interaction network over time, from all mitochondria and all connections (Figure 4A).

We focused on node-specific values, beginning with degree, the number of immediate neighbours of each node i.e. how many other mitochondria did a single mitochondrion meet over the time we tracked it within the cell, or in graphical terms, how many sticks are connected to the circles. Strikingly, the node values for mitochondria with DNA reach much higher local connectivity levels than those without mtDNA (Figure 4). This means that mitochondria with mtDNA have more immediate neighbours (of either type) than those without. The network illustrations (Figure 4Ai-iii), suggest that those without mtDNA are enriched in those with degree 0 (i.e a singleton, circle with no sticks) and those with degree 1 (i.e at the periphery of the network, circle with just one stick). This is confirmed by quantifying the number of nodes with degree 0 or 1 in proportion to the number of nodes of each status at representative time points across all cells analysed (Figure 5). When compared to those of degree 3, i.e with three immediate neighbours (Figure 5C), chosen as it is well represented in both those with and without mtDNA, we see no particular mtDNA status as prominent over frames or cells, in contrast to the over-representation of those without mtDNA in the lowest degree nodes of 0 or 1 (Figure 5A,B). Thus, mitochondria without mtDNA do not have as many immediate neighbours as those with mtDNA, and are more likely to be in nodes with only zero or one immediate neighbour(s).

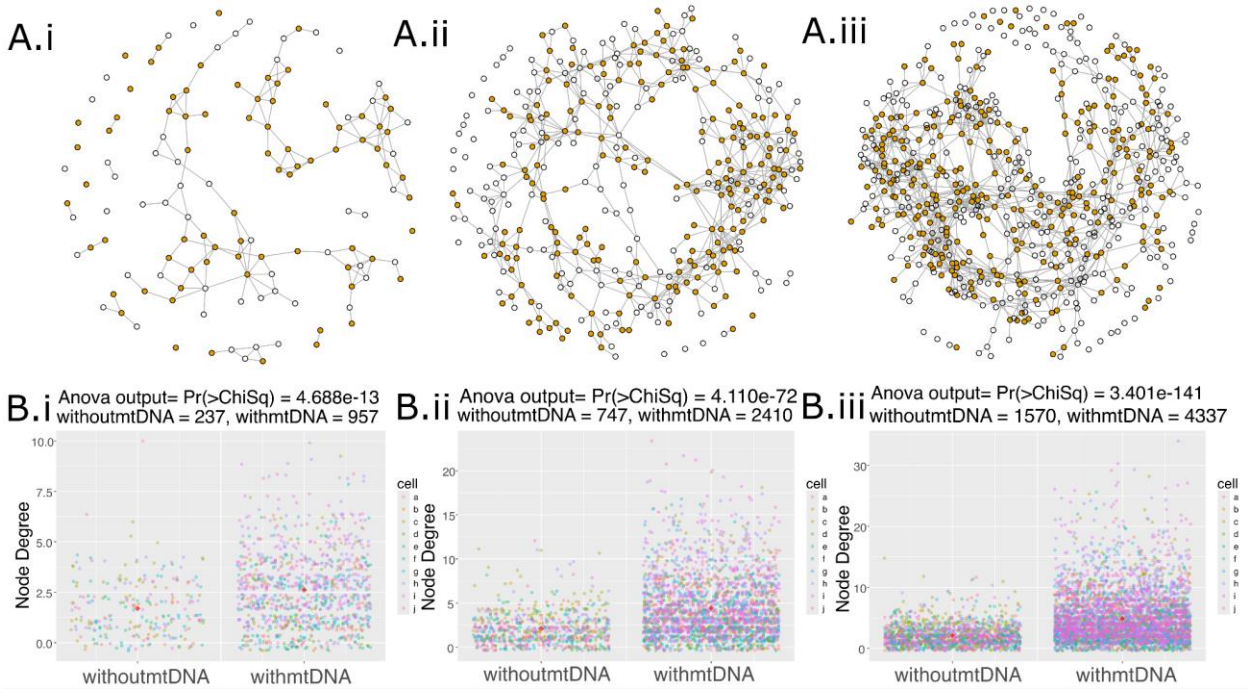

Figure 4: Mitochondria without mtDNA demonstrate lower immediate connectivity. A) representative network of all mitochondrial encounters built up over time, shown at frame 10 (representing 22.1sec of video time) (i), 50 (ii), 109 (iii), colour coded by mtDNA presence (orange) or absence (white), with edges representing close encounters between individual organelles. B) Node degree with mean (red diamonds) for nodes with and without mtDNA over the same frames, and across all 10 hypocotyl cells (a-j). P-values are the outcome of a two-way blocking factors anova (cells as block). Red diamonds represent the mean of all points.

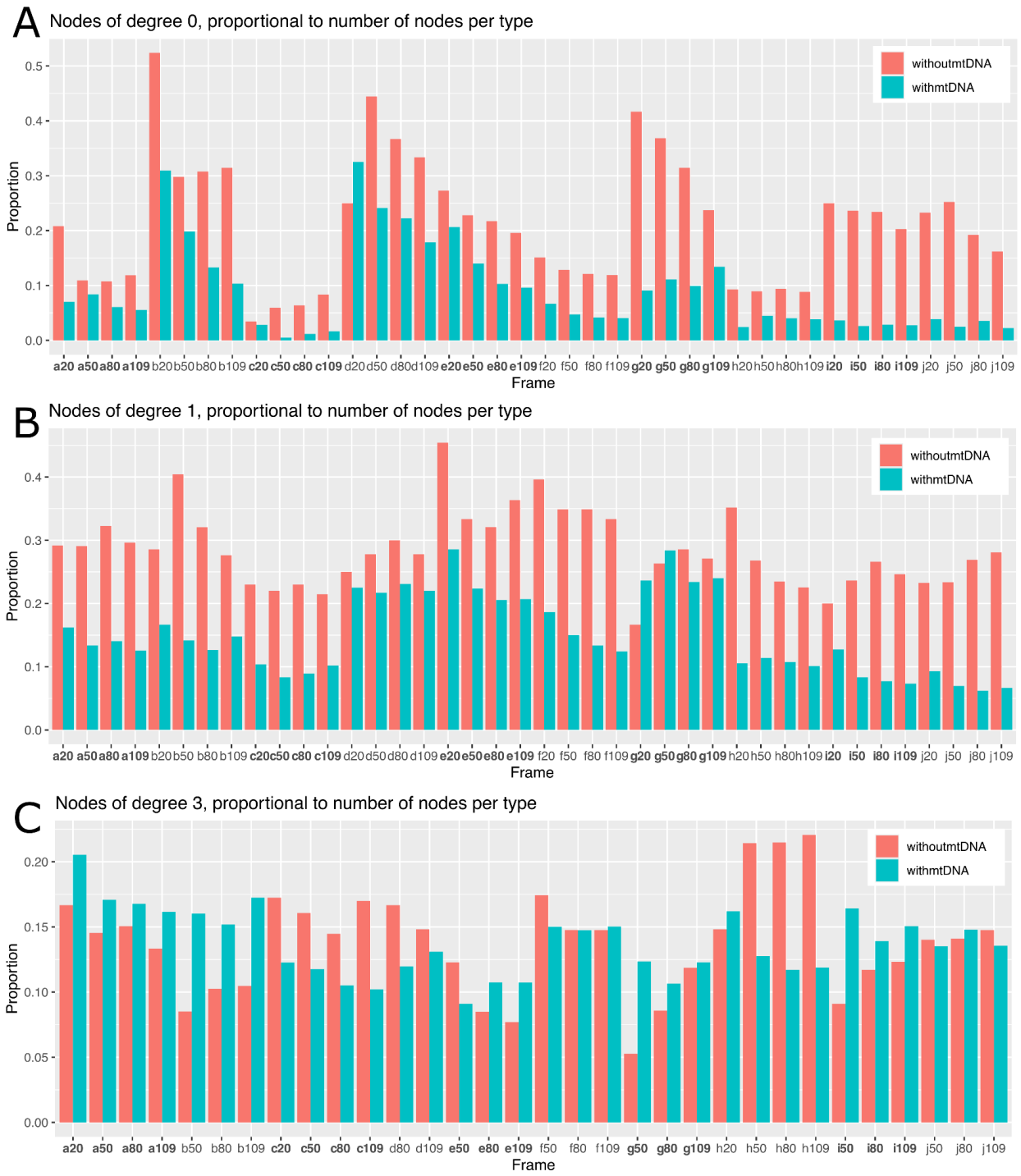

Figure 5:

Number of nodes with degree value A) 0, B) 1, C) 3, proportional to the number of nodes of equal mtDNA status, plotted over n = 10 hypocotyl cells (a-j), and four networks at frames 20, 50, 80 and 109. X axis emboldened to distinguish cells.

Mt-HI-NESS nucleoid binding provides improved visualisation of mtDNA nucleoids in plants

Until now, mtDNA imaging in plants has relied on exogenous stains that face the impermeability barrier of the plant cell wall or fluorescent proteins that are target-specific and do not bind mtDNA ubiquitously. Live rates of mtDNA exchange across mitochondrial populations in plants are also yet to be established. Therefore, a photoconvertible ubiquitous mtDNA marker was sought. We modified the mt-HI-NESS construct developed in human cells for stable transformation and ubiquitous mitochondrial targeting in plants (Deng et al., 2023). This construct relies on the H-NS bacterial nucleoid binding protein attached via a linker to the photoconvertible Kaede protein. We codon-optimised for *A. thaliana* and chose two plant-specific mitochondrial targeting sequences to test, IVD and AOX (see methods). As a further test, we also used the original human Cox8 presequence construct to see if it would function in a plant system.

Initial tests were carried out using the *N. benthamiana/Agrobacterium* transient transfection system (see methods), with IVD and AOX mt-HI-NESS specifically localising *within* the individual mitochondria of epidermal cells (Figure S5D,E), using a red fluorescent IVD-FP611 construct as a mitochondrial marker. Compared to the same tissue using IVD-FP611 and stained with SYBR green, we see a similar nucleoid signal, showing that mt-HI-NESS is ubiquitously staining mtDNA nucleoids (Figure S5B,D,E). Using Cox8-mt-HI-NESS, we observed non-specific chloroplast and nuclear DNA targeting (Figure S5C), presumably because the mitochondrial targeting sequence was not plant-specific.

Following successful testing in *N. benthamiana,* the AOX/IVD-mt-HI-NESS constructs were taken forward. Floral dip of mito-mCherry and Col-0 plants was performed, and positive transformants were isolated. Each combination demonstrated mitochondrial nucleoid specific binding, and here we show mito-mCherry with AOX-mt-HI-NESS (Figure 6A, B) and Col-0 with IVD-mt-HI-NESS (Figure 6D). This binding was

ubiquitous as compared to the same tissue stained with SYBR green (Figure 6C), although exogenously applied SYBR is also visible around the outside of the cell. We did not find any differences in localisation or expression between IVD and AOX mt-HINESS (Video 2,3).

We tested the photoconvertible properties of the Kaede protein under UV laser (405nm), and demonstrated complete green-to-red switching of each mitochondrial nucleoid in a specified region of interest (Video 4).

To investigate if the IVD/AOX-mt-HI-NESS lines impact mitochondrial function through their nucleoid binding, we conducted a series of physiological experiments. We see no difference in the rosette area of transformed *Arabidopsis* (Figure S6A,B). We initially saw a difference in root length, a key phenotype for mitochondrial function, when testing Col-0 against mito-mCherry AOX or IVD-mt-HI-NESS (Figure S6A,B). However, we subsequently tested the mito-mCherry line (into which these constructs had been transformed) against Col-0 and saw the same shorter root phenotype (Figure S6C,D). Therefore, the difference in root length is determined to be due to the mito-mCherry background, and not the mt-HI-NESS nucleoid binding protein. We next performed oxygen consumption assays on leaf discs of the same three genotypes, finding no difference in oxygen consumption rate between them (Figure S6E). Finally, to determine whether the mtDNA binding ability of mt-HI-NESS disrupted expression of key genes, we used immunoblotting to assay the mitochondrial proteins Cox2 and AtpB using nuclear (Histone H3) and chloroplast (PsbA) proteins alongside as controls. We saw no differences between loading controls and signal across genotypes tested (Figure S6F). We also note that during the development of the mt-HI-NESS lines in human cells, no transcription alterations were observed (Deng et al., 2023).

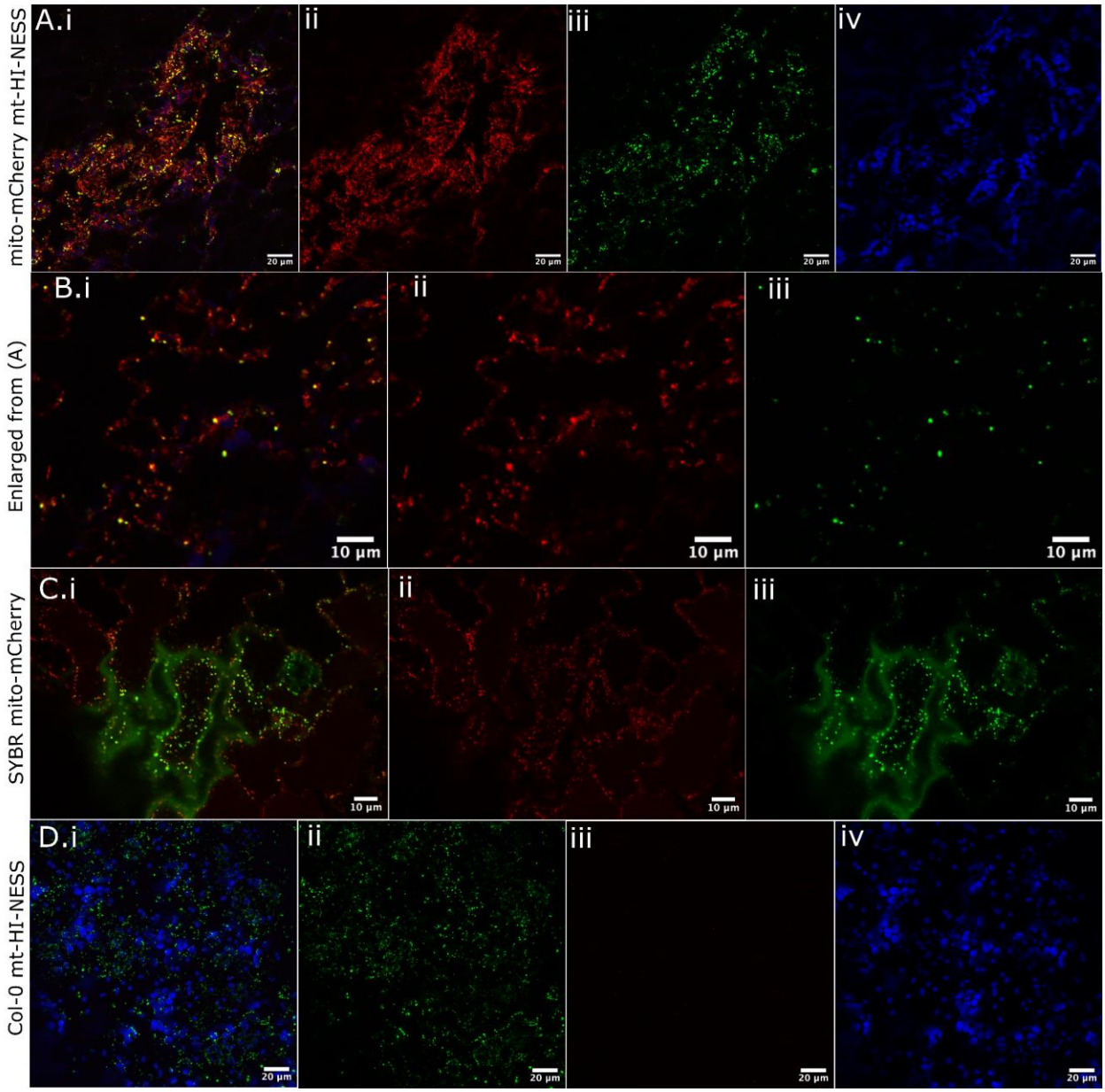

Figure 6:

Mt-HI-NESS stable *Arabidopsis* transformants in mito-mCherry or Col-0 backgrounds demonstrate mitochondrial nucleoid localisation. A) Merged (i) maximum intensity projection (10 frames, 0.5µm step) with mito-mCherry (ii, red), AOX-mt-HI-NESS non-photoconverted Kaede (iii, green) and chlorophyll autofluorescence (iv, blue). B) Enlarged view of a single z-slice of same image, tiles as before. C) Single frame of mito-mCherry (red, ii), stained with SYBR Green (green, iii). D) Merged (i) Maximum intensity projection (57 frames, 0.8µm step) of Col-0 IVD-mt-HI-NESS (ii, green) with no mito

marker (iii, red), and chlorophyll autofluorescence (iv, blue). All images were taken from abaxial epidermal leaf cells of mature Arabidopsis (~2-3 weeks).

Discussion

Mitochondria in plant cells are highly dynamic and have many varied functions, including the generation of ATP via the electron transport chain. The most energetically and physically central proteins to this process are encoded in the mitochondrial genome, which is organised into highly variable and recombinationally active nucleoids distributed throughout the mitochondrial population. We demonstrate here a difference in both physical and network (or 'social') dynamics between those that carry these nucleoids, and those that do not.

Mitochondria without mtDNA have an increased intermitochondrial distance, that is, they are further apart from every other mitochondrion on average than those with mtDNA. In addition, mitochondria without mtDNA, during the time we imaged them, travel a smaller area around the cell than those with mtDNA. We see no differences in speed between those with and without mtDNA. However, speed did also not significantly differ in mitochondria with compromised mtDNA repair machinery (Chustecki et al., 2022). Mitochondrial motion in plant cells is driven by myosin motors on actin filaments (Avisar et al., 2008, 2009; Sparkes et al., 2008; Zheng et al., 2010), and by cytoplasmic streaming which is a consequence of organelle motion (Shimmen and Yokota, 2004; Peremyslov *et al.*, 2015; Tominaga and Ito, 2015). It may be that functional differences in mitochondria, including the presence of mtDNA do not alter this cellular machinery, and therefore do not alter the speed.

'Empty' mitochondria do not have as many close connections (have a lower degree) as those with mtDNA, across any frame time, and are more likely to have 0 or 1 immediate local neighbour than those with mtDNA. Encounters between mitochondria are necessarily driven by their physical dynamics, and this behaviour correlates with the physical measurements we see for those without mtDNA.

The connection between absence of mtDNA and behaviour is difficult to disentangle. Our initial hypothesis was that empty mitochondria would make more

connections with other mitochondria, in order to fuse and acquire DNA. This might happen, but we were unable to observe it, possibly because the time frame of 4 minutes is too short to see such events. Longer time frames were not done to avoid issues of photobleaching the fluorescent dyes, and the plant cells becoming hypoxic under the cover slip. Why then, do empty mitochondria make fewer connections with other mitochondria? They may still be looking for partners for fusion, but mitochondria with DNA may vary in their receptivity to fusion with an empty partner, perhaps depending on how much of the genome they carry.

Here we show that empty mitochondria cover less area within the cell- why is this? They move at the same speeds, so this difference cannot be due to a difference in binding to the myosin motors between mitochondria with and without DNA, but other external partners besides myosin could be involved. In animal mitochondria there is evidence of a link between ATAD3 proteins, which we now know as involved in plant mitochondrial nucleoid organisation, and the function of protein complexes at the mitochondrion-ER interface (Baudier, 2018; Kim et al., 2021). There is increasing evidence of the role of the ER in regulating mitochondrial fission and fusion (Mueller & Reski, 2015; White et al., 2020), and future research will be necessary to determine if there is indeed a link between mitochondrial nucleoids, organelle dynamics and cellular players in these interactions.

An additional question is why there is a persistent subpopulation of empty mitochondria. One hypothesis for this may be that those without mtDNA are targeted for degradation, and as a consequence, are also excluded from the connectivity enjoyed by the rest of the individuals in the network. However, a population of ‘empty’ mitochondria is present across all cells and both cell types tested here, as well as in all non-reproductive plant tissues where mtDNA has been imaged (Arimura *et al.*, 2004; Sheahan, 2005; Kim *et al.*, 2021). How then, is this population maintained, whether active or accidental? Over the course of 2 hours in onion epidermal cells, mitochondrial contents can be completely homogenised, and during fission events mitochondria without nucleoids can be generated (Arimura et al., 2004). Upon full fusion of mitochondria, mtDNA molecules are evenly spaced over the network in plant protoplasts (Sheahan 2005). Thus it remains curious that this population of empty

mitochondria persists. The gain and loss of mitochondrial DNA within the population of mitochondria in a single cell is clearly a very active and dynamic process, worth further study. We know little about mtDNA homogenisation and exchange in non-reproductive tissues, and tools such as the photoconvertible mt-HI-NESS probe developed here will help us investigate further.

In non-reproductive cells, the maintenance of organellar DNA is reduced or eliminated, resulting in overall loss of DNA in older cells (Kumar et al., 2014; Oldenburg & Bendich, 2015). To avoid this potential problem, our experiments used very young plants, including leaf epidermal cells that will form much larger rosette leaves and will be metabolically active for another two months. Furthermore the previously described effect of an *msh1* mutant on mitochondrial dynamics shows that the plant is still maintaining organellar DNA with nuclear-encoded repair proteins in these cell types and stages (Chustecki et al., 2022). For these reasons, we do not think there is organellar DNA abandonment or decay in these experiments.

Defining whether a given mitochondrion has DNA or not using the continuously varying signal of SYBR Green fluorescence is challenging. Tracking multiple shapes over time in video data using more than one channel as input is also a non-trivial problem in practice (Hänselmann & Herten, 2017; Qiang et al., 2017; Spilger et al., 2022). Many tools designed to quantify mtDNA have been developed in human or yeast cells, where mitochondria form reticulated lengths, or in only single frame images (Kukat et al., 2011; Rey et al., 2023). We took several approaches to define ‘with and without DNA’ and chose the strategy resulting in the least data loss while avoiding false positives. It is also possible to define single time points in each video as present/absent, negating the trajectories definitions of lenient/tolerant/strict, and although we did not include this analysis here, we could not find evidence of DNA exchange from a mitochondrion with mtDNA to one without. This may be because the imaging time (~4 minutes) was not long enough to locate these events. It may also be that ‘empty’ mitochondria do not often receive nucleoids from their neighbours.

It has been demonstrated that fusion requires a potential across the inner membrane in plant protoplasts (Sheahan 2005), and that mitochondrial fusion apparatus adapts in response to changes in membrane potential, at least in mammalian cells

(Herlan et al., 2004; Twig et al., 2008). Therefore, it could be the case that those without mtDNA do not have the machinery to maintain membrane potential, therefore reducing their ability to fuse. This raises the question, how do mitochondria without mtDNA keep their protein apparatus, subject to constant degradation, healthy enough to participate in this process of fusion and fission? The answer is most likely the exchange of other gene products, or whole membrane protein complexes and RNAs, during transient close proximity and full fission and fusion events, rather than the requirement to carry mtDNA at all times (Giannakis, 2022). Analysis of other functional molecules and their exchange or homogenization over these timescales would allow investigation of this, as well as analysis of any correlation between membrane potential and mtDNA presence/absence, or the establishment of functional subpopulations of these organelles (Kuznetsov *et al.*, 2006; Logan, 2006; Kuznetsov *et al*. 2009; Fuchs *et al.*, 2016; Willingham *et al.*, 2021).

Most plant cells do not readily take up exogenously applied stains and dyes, requiring long stain times and high dye concentrations to be successful. Exogenous DNA stains are nonspecific, staining chloroplast and nuclear DNA, and can intercalate DNA molecules, impacting replication (Prole, 2020; Deng *et al.*, 2023). We sought a ubiquitous, specific and non-intercalating marker for mtDNA in plant cells. The DNA binding protein TFAM has been used for this in human and yeast cells, however plant cells lack it and overexpression can impact mtDNA function (Alam et al., 2003; Kukat et al., 2011). Other DNA-binding proteins in plants are repair proteins, found in very low numbers per mitochondrion (P. Fuchs et al., 2020). Nucleoid organising proteins in plant mitochondria can have preferential binding sites across the genome (Kim et al., 2021). We therefore were inspired by the work of (Deng et al., 2023), implementing the bacterial H-NS nucleoid binding protein, to bind each and every nucleoid in mitochondria. We confirmed that this nucleoid binding protein does not impact growth or respiration in *Arabidopsis*, and its photoconvertible nature can be used in future experiments to track the movement, and colocalisation of mtDNA nucleoids originating in different individual organelles. This novel fluorescent protein construct will be particularly useful for imaging meaningful exchange of mtDNA nucleoids across all

tissue types, elucidating further the role of mitochondrial dynamics on DNA maintenance and exchange.

We have shown that the complex physical and network behaviours of plant mitochondria are linked to whether the mitochondrion contains DNA or not. Mitochondrial motion is very costly in terms of the cell's energy budget (each myosin step is estimated to use about 1 ATP for every 35nm travelled (Tominaga et al., 2003), and they can move at speeds of up to 10µm/s (Zheng et al., 2009)), suggesting the importance of this dynamic motion for cellular function. Much of the motion may be related to acquiring substrates and delivering products to different parts of the cell, and to and from other bioenergetic organelles. Individual mtDNA content is another parameter that affects their behaviour. The persistence of empty mitochondria and the factors connecting the presence of DNA to the outer membrane where movement is mediated are important remaining mysteries.

<u>Supplementary material</u>

Video 1: Time lapse video of SYBR stained hypocotyl cell of 5-day old *Arabidopis* seedling. Frame interval = 2.21 secs, Exported at 10 fps. Green channel- SYBR signal (mtDNA). Red Channel - mito-mCherry signal (mitochondria).

Video 2: IVD-mt-HI-NESS timelapse. Time-lapse video of leaf epidermal cells of 2-3 week old mito-mCherry *Arabidopsis* stably transformed with IVD-mt-HI-NESS, Frame interval = 3.28 secs, exported at 10 fps. Green; IVD-mt-HI-NESS signal (mtDNA), Red Channel; mito-mCherry signal (mitochondria), Blue; Chloroplast autofluorescence,

Video 3: AOX-mt-HI-NESS timelapse. Time-lapse video of leaf epidermal cells of 2-3 week old mito-mCherry *Arabidopsis* stably transformed with AOX-mt-HI-NESS, Frame interval is 6.06 secs, exported at 10 fps. Green; AOX-mt-HI-NESS signal (mtDNA), Red Channel; mito-mCherry signal (mitochondria), Blue; Chloroplast autofluorescence,

Video 4: IVD-mt-HI-NESS photoconversion time-lapse. Time-lapse of photoconversion from green to red of IVD-mt-HI-NESS (mtDNA marker) in Col-0 *Arabidopsis* epidermal leaf around 2-3 weeks old with no mitochondrial marker. The first frame shows the region hit by a 405nm laser, frame interval is 2.15 secs, and there is a 5 secs gap between frames 3 and 4 when the laser was applied. Total time elapsed 95 secs. Exported at 2 fps.

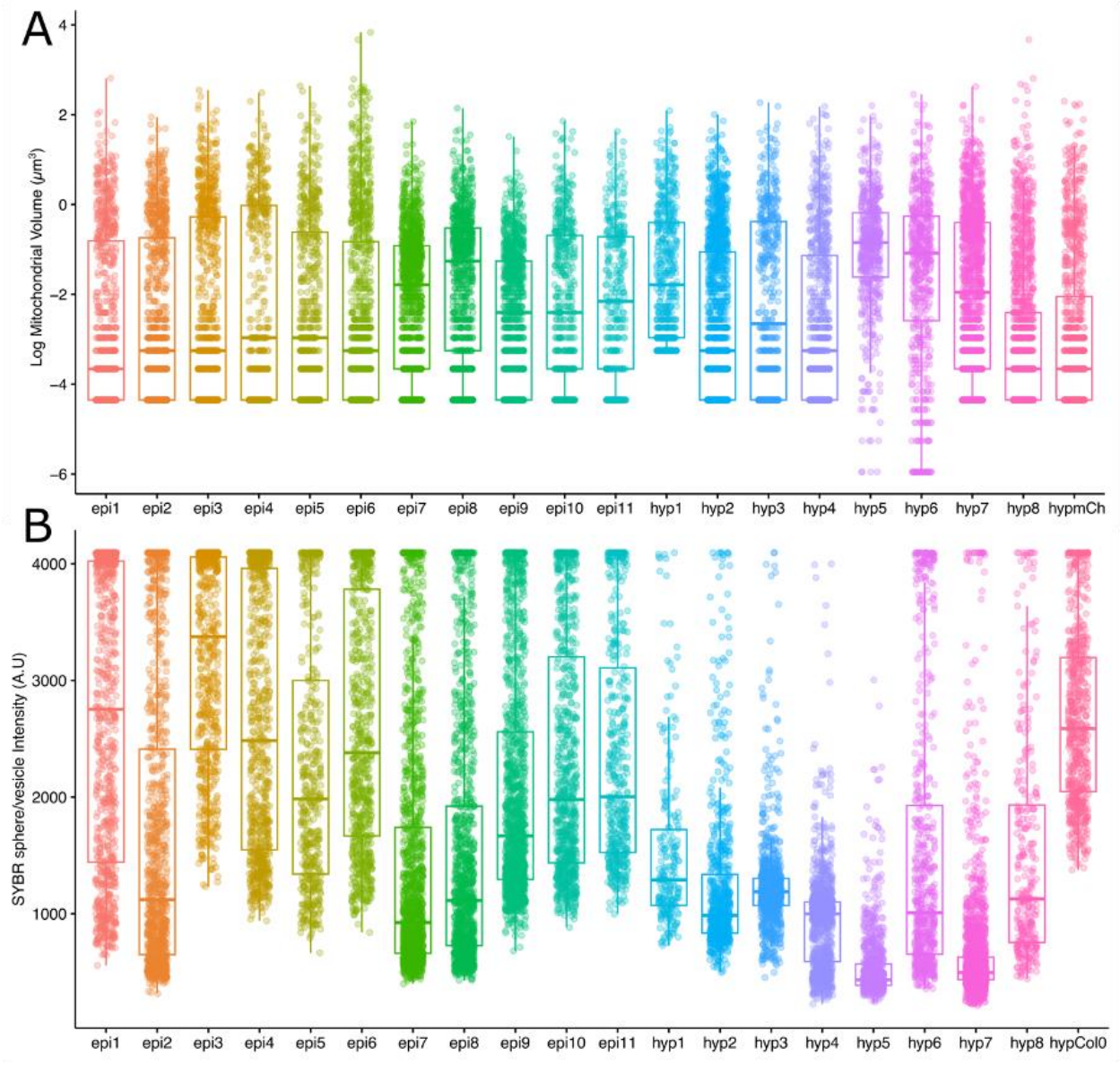

Figure S1: Statistics from fixed, SYBR stained leaf epidermis n = 11, hypocotyl = 8 cells and controls. A) Log mitochondrial volume (µm^3) extracted from fixed mito-mCherry cells compared to n = 1 hypocotyl from an unstained mito-mCherry seedling. B) Intensity of segmented SYBR spheres (representing the mean intensity of all voxels in the sphere) from fixed mito-mCherry cells, compared to n = 1 stained Col-0 hypocotyl (no mitochondrial marker).

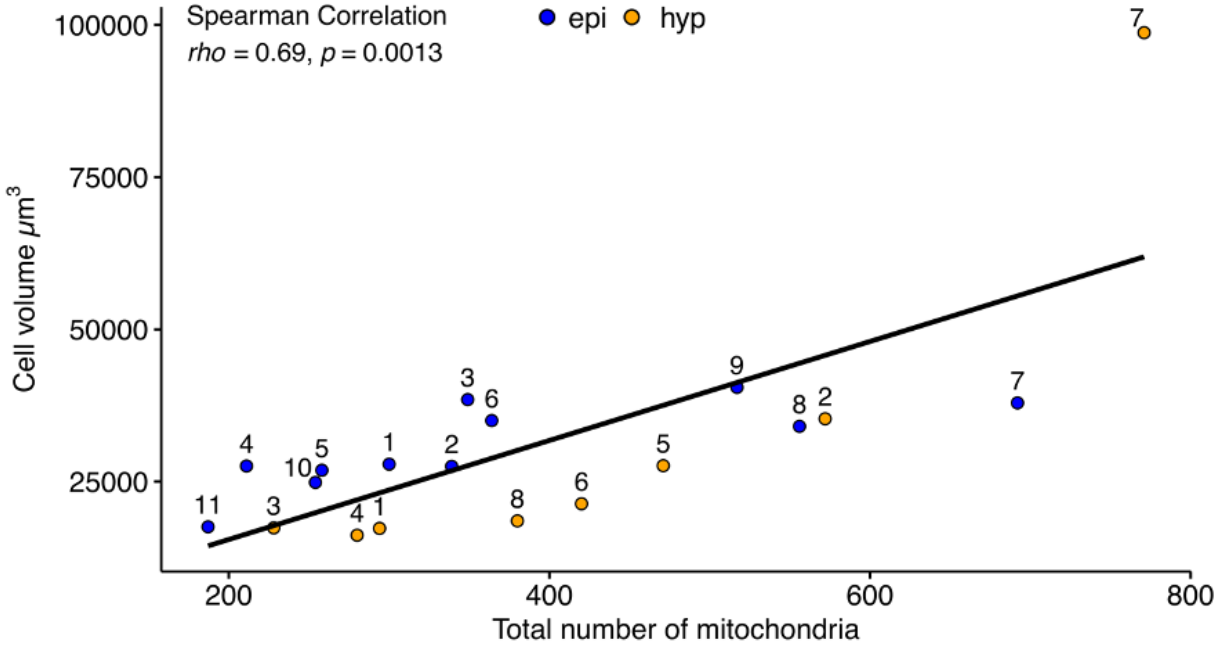

Figure S2: Spearman correlation between cell volume and total mitochondrial number, across the two cell types used (leaf epidermis n = 11, hypocotyl n = 8), with a linear regression line added.

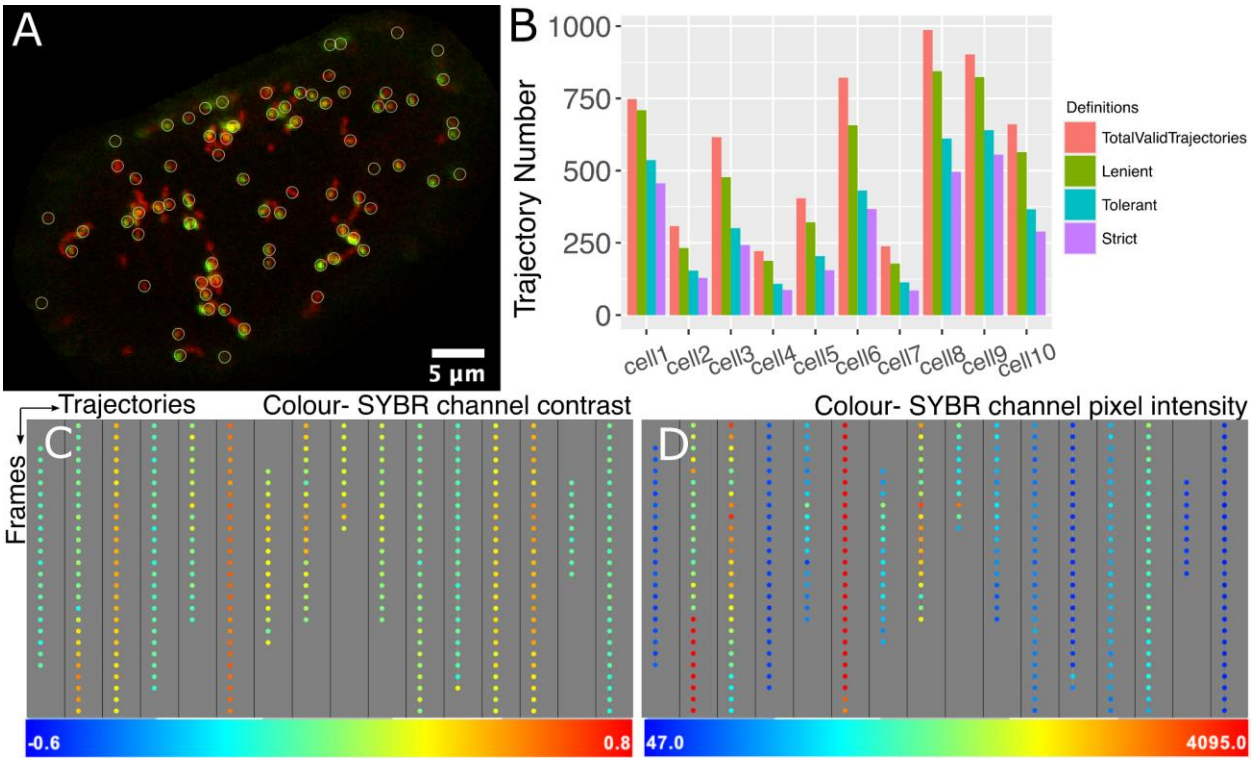

Figure S3: Detecting and defining mtDNA presence using contrast. A) Single *Arabidopsis* hypocotyl cell with mito-mCherry marker, stained with SYBR green, still frame from time-lapse, with detected mitochondria (red) using Trackmate (white circles, diameter 1.1µm), showing only those that passed the chosen Contrast threshold for this time-lapse. B) Quantification of trajectory number over total, alongside three definitions of mtDNA presence, in order of strictness, across 10 single hypocotyl cells. C,D) Trackschemes, from Trackmate (Tinevez *et al.*, 2017) showing multiple trajectories (across), made up of points at each time frame (down), colour coded by contrast value of SYBR channel (C), or pixel intensity values of SYBR channel (D). Lower values = blue, higher values = red.

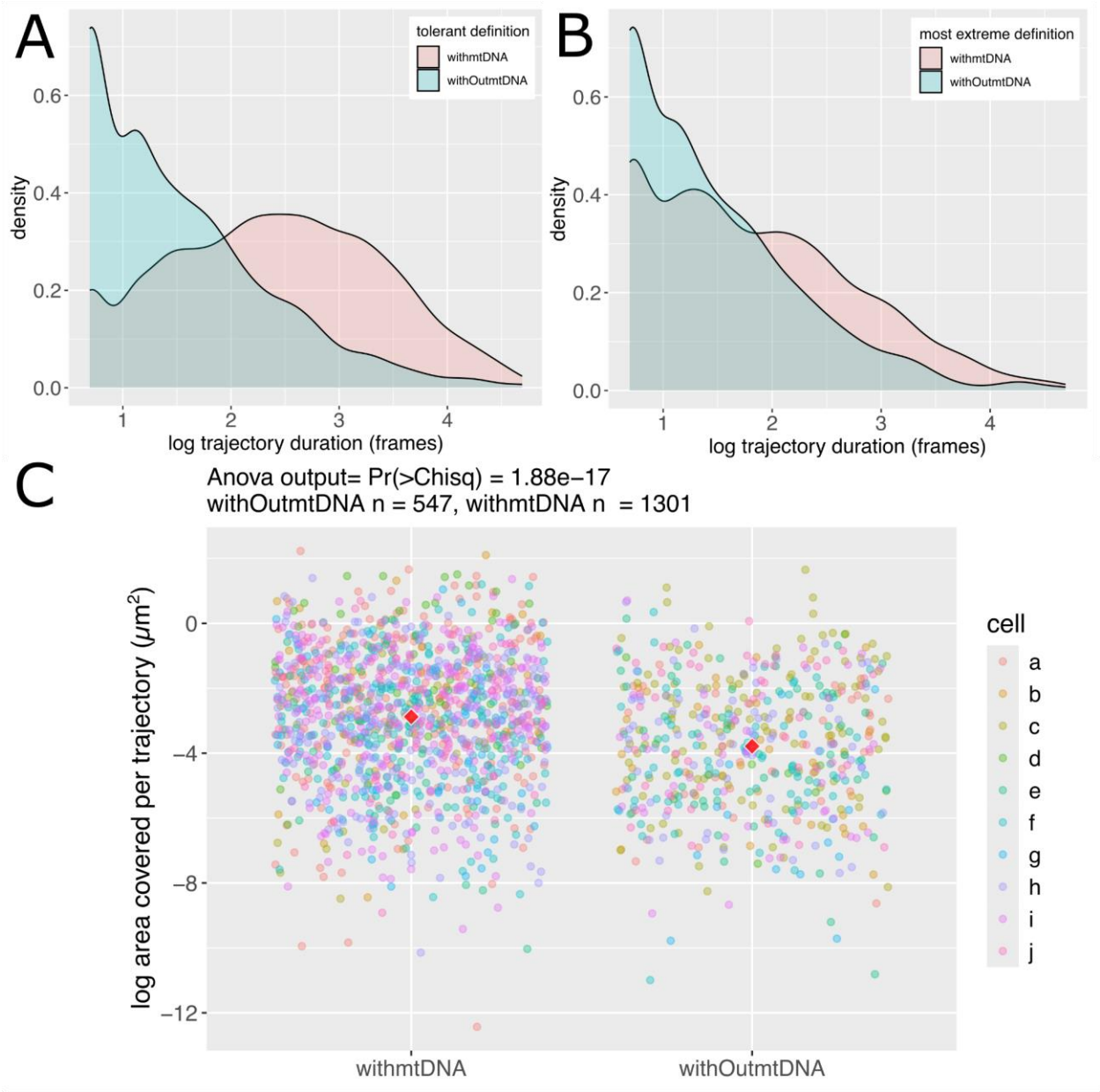

Figure S4: Impact of differing mtDNA presence definitions on area analysis. Comparing trajectory duration in frames between trajectories defined as without (blue) or with (pink) mtDNA according to a 'tolerant' (A) or 'strictest' (B) definition. C) Impact of *most extreme* implemented definition of mtDNA presence on differences in cell area travelled by trajectories (μm^2). P-value is the outcome of a blocking factor Anova (cells as block). Red diamonds represent the mean of all points.

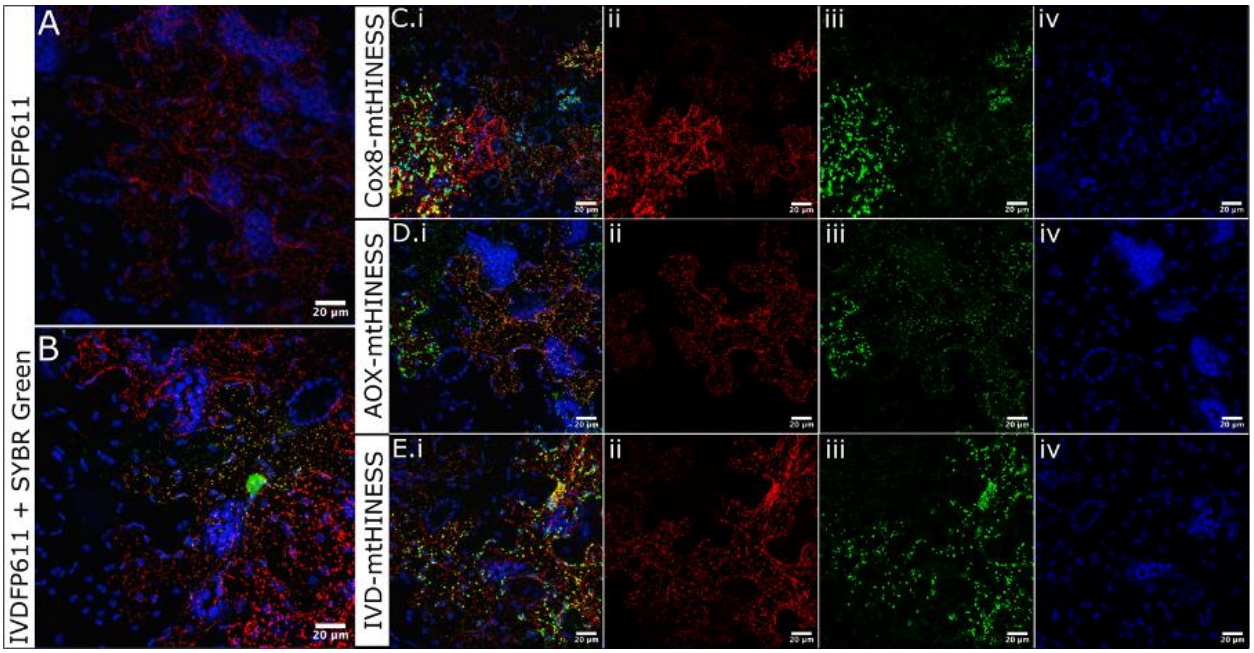

Figure S5: Validation of mt-HI-NESS nucleoid reporter constructs in *N. benthamiana* transient infiltrations, abaxial epidermal cells. A) Expression of IVD-FP611 control for mitochondrial signal (red) and chloroplast autofluorescence (blue). B) Expression of IVDFP611 mitochondrial localised fluorescent protein (red) subsequently stained with SYBR green (green), with chloroplast autofluorescence (blue). C-E) Merged (i) coinfiltrations of IVDFP611 (ii, red) with mt-HI-NESS constructs (iii, green) differing by mitochondrial targeting sequence Cox8, AOX, IVD respectively, with chloroplast autofluorescence also shown (iv, blue).

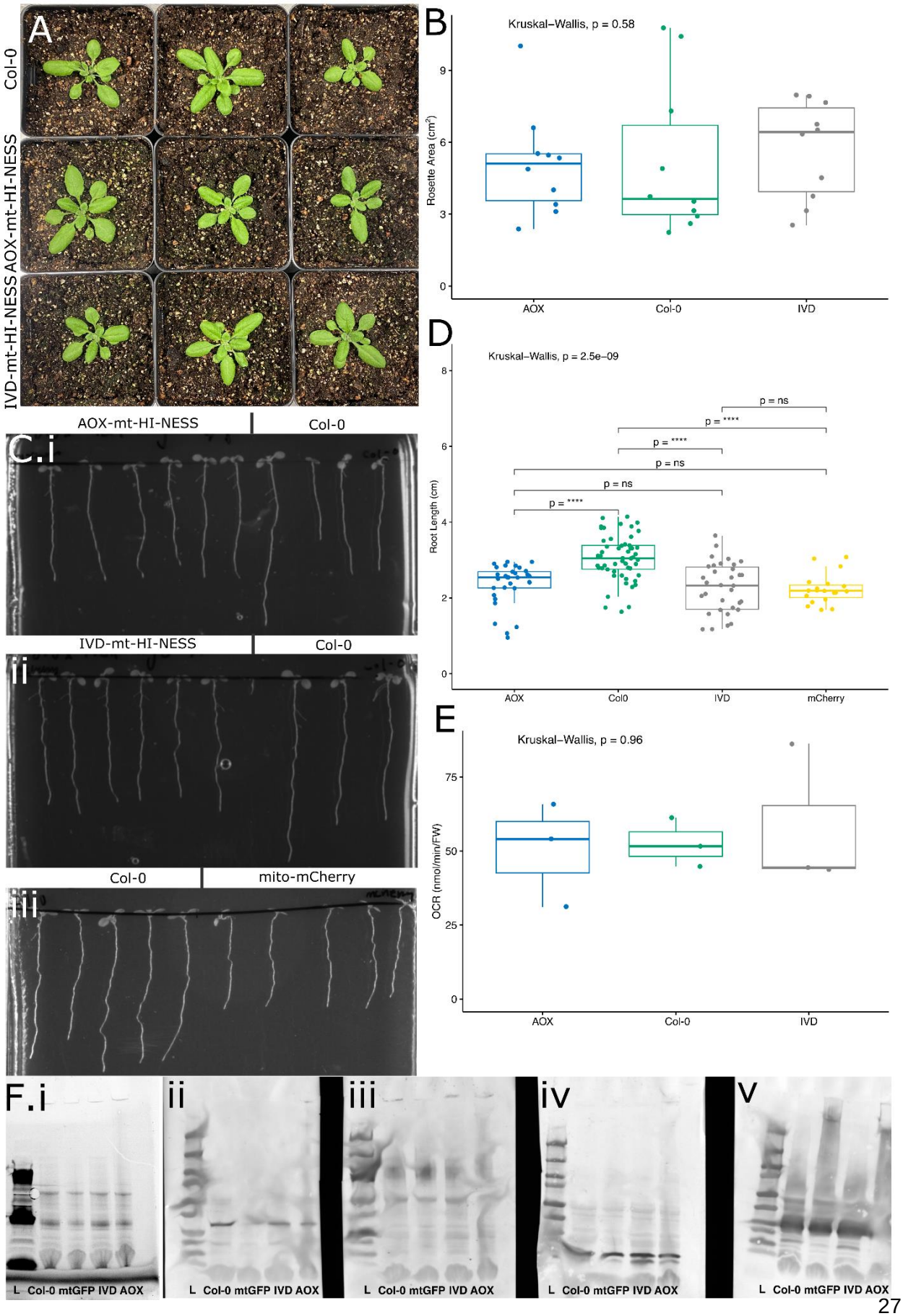
A
Col-0
AOX-mt-HI-NESS
IVD-mt-HI-NESS
B
Kruskal–Wallis, p = 0.58
Rosette Area (cm²)
AOX
Col-0
IVD
D
Kruskal–Wallis, p = 2.5e–09
Root Length (cm)
p = ns
p = ****
AOX
Col0
IVD
mCherry
E
Kruskal–Wallis, p = 0.96
OCR (nmol/min/FW)
AOX
Col-0
IVD
C.i
AOX-mt-HI-NESS
Col-0
ii
IVD-mt-HI-NESS
Col-0
iii
Col-0
mito-mCherry
F.i
ii
iii
iv
v
L Col-0 mtGFP IVD AOX

Figure S6: Physiological validation of mito-mCherry mt-HI-NESS *Arabidopsis* stable transformants. For brevity, in this figure AOX= mito-mCherry AOX-mt-HI-NESS, IVD = mito-mCherry IVD-mt-HI-NESS. A) Rosette images of Col-0 WT, AOX and IVD, n=3 B) Rosette area analysis between the same genotypes as in (A), where n=10 for each line. C) Root growth assays comparing AOX and Col-0 (i), IVD and Col-0 (ii), and Col-0 and mito-mCherry (iii). D) Quantification of root length (cm) across the four lines seen in (C), AOX n=32, Col-0 n= 54, IVD n= 34, mito-mCherry n=19. E) Oxygen consumption rate (OCR) in (nmol/min/FW) across Col-0 WT, IVD and AOX. F) Immunoblots of Col-0, mtGFP, IVD, and AOX detecting mitochondrial, nuclear and chloroplast proteins showing gel loading control (i), CoxII (mitochondrial, ii), AtpB (mitochondria, iii), H3 (nuclear, iv), PsbA (chloroplast, v), L = ladder. *P*-values represent Kruskal–Wallis test outcomes across all genotypes, and pairwise *P*-values are false discovery rate-adjusted outcomes of a post-hoc Dunn test, ****= p< 0.001, ns = not significant. Boxplots represent the median and 25th/75th percentile, with whiskers showing the smallest/largest value within 1.5× the interquartile range.

Methods

Data and Code availability

-Videos 1-4 are available at github.com/jo-c-bio/physical-genetic-dynamics
-All code generated for this paper is also available at the link above, as are the scripts used to generate figures for this paper.
-Final plasmid sequences of AOX-mt-HI-NESS, IVD-mt-HI-NESS and Cox8-mt-HI-NESS are also available at the link above.

Video Analysis

Video analysis closely follows (Chustecki *et al.*, 2021). Time-lapse videos of SYBR stained mito-mCherry hypocotyl cells of 5-days old *Arabidopsis* were cropped to single cells using extracellular SYBR signal. 8 videos were taken, from which 10 unique cells were analysed (n=10). Ensuring resolution (4.83 pixels/µm) and time steps (2.21 secs) were consistent across the videos analysed, Trackmate v7.11.1 (Tinevez et al., 2017) in ImageJ v2.14.0 was used to track movement in the mCherry channel only. Typical settings were using the LoG Detector filter with blob diameter of 1.1µm, a threshold of 76-100, and a quality filter on spots if necessary of between 87-180. Then, the Simple LAP Tracker was applied with a linking max distance of 2.5, gap-closing distance of 3.5, and 2 frames used for gap-closing. Manual editing of tracks was undertaken if deemed necessary.

Full .xml files were exported, and imported into RStudio (v2024.04.0+735) using the TrackmateR package (v0.3.10) (Royle, 2024), to include all spot statistics. To define trajectories as having or not having mtDNA, we use the second channel of the SYBR signal, and two definitions- Contrast and Maxima. Contrast is calculated as the Intensity (A.U) of pixels inside the spot radius (r) compared to outside as defined by $2r$ by $(I_{in}-I_{out})/(I_{in}+I_{out})$, and for each cell, the contrast cutoff for what counted as a candidate SYBR signal was manually selected using the visualisation tool and spot pseudo-colouring in Trackmate. Cutoffs ranged from 0.05-0.22 contrast values, where anything below was without mtDNA, and anything above was with mtDNA.

For Maxima definition of mtDNA presence, the FindMaxima (Wagner, 2016) function in ImageJ was run through a macro, across three frames (1,50,100) of each video, and looped over prominence values in increments of 50 from 150-500, with the ‘strict’ setting applied. Final prominence values used across the videos ranged from 200-400. Images with maximum points as crosses were viewed to choose representative best prominence value for true SYBR signal, and this chosen prominence value was used for each video to generate a list of pixel coordinates from puncta that were SYBR signal. After conversion to microns to match Trackmate output, the R point.in.polygon function from sp package v2.1-4 was used to assess whether or not the maxima puncta sat inside a Trackmate spot from the mito-mCherry signal. If it

did, the mitochondrion at that frame has mtDNA according to our Maxima definition, and if not, it was without mtDNA.

For both Maxima and Contrast definitions, three strictness definitions were then defined. Each video had its own contrast and prominence value. We define the first as *Lenient* in that only one frame in the entire trajectory needs to be above the threshold value to pass (as this mitochondrion having mtDNA). The next is *tolerant*, where at least two adjacent frames must be above the threshold to pass. The last definition is *strict*, where at least three adjacent frames must be above the threshold to pass. .

We characterise encounter networks as undirected edges between nodes representing mitochondria. Edges are built when mitochondria are within 1.6µm of each other, and do not represent fusion events. Encounter networks build as frame times progress, and network build-up is historical. Node degree is then calculated as the number of immediate neighbours each node is connected to. This analysis aimed to investigate connectivity values for nodes with and without a characteristic, therefore we did not implement global values of connectivity for entire networks, as we analysed connectivity between individual nodes, instead of between whole networks, and avoided splitting the network into subgraphs. R packages iGraph (v2.0.3) and brainGraph (v3.1.0) were used to calculate network statistics and visualise networks.

<u>Plant growth</u>

Seeds of Col-0, mito-mCherry, mCherry-MTHINESS, Col0-MTHINESS, mtGFP-MTHINESS lines were surface sterilised using 50% (v/v) household bleach solution with continual inversion before washing three times with sterile ddH_2O, and plating onto ½ MS agar with 5µg/mL Nystatin at pH 5.7 before stratification at 4˚C for two days in the dark. Seedlings were either grown to 4-5 days old in ½ MS before use or transplanted to Berger BM2 germinating soil with Turface MVP. Any plants grown on soil were grown at 22˚C in 8 hrs dark, 16 hrs light.

N. benthiamiana plants were grown in greenhouse conditions with supplemented light 12hrs a day and temperature ranges at 27-24˚C daytime and 21-19˚C night time from seed until ~3-4 weeks old.

Plant tissue fixation staining and imaging

5-days old *A. thaliana* seedlings were fixed in 3.5% paraformaldehyde (EMS, #15710) in PBS buffer (Gibco, #10010023) for 30 mins, ensuring complete submersion by applying gentle vacuum pressure to the solution. Seedlings were washed with PBS before further staining.

SYBR green (invitrogen, #S7563) was used at a 1:1000 dilution in ddH_2O, and 5-days old *A. thaliana* seedlings were stained for 45 mins before washing in PBS or H_2O and use.

All laser scanning confocal micrographs were taken on an upright Nikon A1-NiE system (RRID:SCR_020318) using NIS-Elements Confocal image acquisition and analysis software, using a 60x water objective. Images were taken using a sequential channel series setting, to minimise cross-channel signal, and the channels used were: GFP, Ex: 488nm, Em: 525 (500-550), TxRed, Ex 561, Em: 595 (570-620), Cy5, Ex: 640nm, Em: 700 (663-738).

All time-series images used have a frame time of 2.21s. For imaging of live hypocotyl cells, and fixed hypocotyl and leaf epidermal cells, 5-days old seedlings grown on plates were used. For mt-HI-NESS leaf epidermal images, ~2/3 week-old plants were used. Tissues were mounted in water on glass slides, with double sided sticky tape and a glass cover slip.

For photoconversion of the Kaede fluorescent protein of the AOX/IVD-mt-HI-NESS lines, the A1 and ND Stimulation features of the NIS-Elements were used to target 4% of the total field of view for 5 seconds at 10% of 20mW LD 405nm laser power. Frame intervals were 2.15secs and the total time imaged was 95 secs.

Cell segmentation with IMARIS

Z-stack files of fixed cells were imported into IMARIS (version 10.1.0). The cell feature was used to define thresholds for segmenting vesicles (mitochondrial DNA puncta) and nuclei (mitochondria). The cell outline segmentation was not implemented, as a reliable

cell wall/membrane stain could not be implemented. To work around this, manual cropping of cell outlines based on SYBR stain at the cell wall was performed in ImageJ2 (2.14.0/1.54f) before import. Further cropping was done using cropping planes in IMARIS, until a clear view of a single cell in each case was achieved. In most cases, the same thresholding parameters were used, briefly: Nucleus Smooth Filter Width = 0.2µm, Nucleus Background Subtraction Width = 0.25-0.4 µm, Nucleus Manual Threshold Range: 77.3-261.3, Vesicle Estimated Diameter = 0.600 µm, Vesicle "Quality" above range: 63.5-207. The hypocotyl hyp1 sample also had an extra filter of "Nucleus Number of Voxels" above 2.05.

During analysis of exported data, any segmented mitochondrion < 0.1µm^3 was removed. SYBR signals from the nucleus and chloroplasts were avoided by quantifying only mtDNA puncta within segmented mitochondria.

Correlation Analysis

Spearman correlation was calculated using the cor.test function of the stats (version 3.6.2) R package, using Spearman's *rho* statistic, for a rank-based association between values, and which uses p-values computed using algorithm AS 89, set out in (Best and Roberts, 1975).

mtHINESS plasmid construction

The mt-Kaede-HI-NESS construct was kindly provided by Professor Timothy Shutt, University of Calgary, developed for use in U2OS human cells, using cox8 as the MTS (mitochondrial targeting sequence). This construct was transformed into TakaraBio Stellar *E. coli* cells (TakaraBio, #636763) and grown on LBA plates with Ampicillin (100µg/mL).

Plasmid DNA was extracted using a column-free plasmid prep method (Green & Sambrook, 2012), and mt-Kaede-HI-NESS-HA was amplified from the plasmid (linearised using AvrII restriction enzyme (NEB, # R0174S) using RP (5'-CAAGAAAGCTGGGTTTAAGCG-3') and FP2 primers (5'- CACCGCCACCATGTCCGT-

3') resulting in only one cox8 sequence being carried through, and a CACC sequence for directional TOPO cloning being introduced. This 1003bp PCR product was extracted from a 1% agarose gel using the TakaraBio gel extraction kit (TakaraBio, #740609.50), and introduced to the pENTR TOPO cloning vector (Kan^R) (Invitrogen, #K240020) which contains the attL1 and attL2 sites LR clonase reactions, and transformed into OneShot Top10 competent *E.coli* (Invitrogen, #C404003).

In parallel, the cox8 MTS was switched for the plant-specific AOX or IVD MTS, and AOX/IVD-mt-Kaede-HINESS-HA constructs were synthesised by ThermoFisher GeneART (https://www.thermofisher.com/us/en/home/life-science/cloning/gene-synthesis/geneart-gene-synthesis.html), following codon optimisation for *A. thaliana* using the VectorBuilder Optimisation tool (https://en.vectorbuilder.com/tool/codon-optimization.html), and with attL1 and attL2 sites introduced for the LR clonase reaction into *Agrobacterium*. These were shipped in pMA-RQ plasmids (Amp^R), and were transformed into TakaraBio Stellar *E. coli* cells, before plasmid DNA extraction.

The three plasmid types, cox8/AOX/IVD-mt-Kaede-HINESS-HA were inserted into separate pUBDEST vectors via the LR clonase reaction ($Spec^R$) (Invitrogen, #1791020), transformed into Top10 competent *E.coli,* sequenced and verified. After one final plasmid prep, they were all transformed into *A. tumefaciens* strain C58C1 for use in infiltration and floral dipping. At each step, plasmids were sequences using Eurofins Genomics whole plasmid sequencing service.

Transient infiltration of *N. benthiamiana*

C58C1 *A. tumefaciens* lines were grown in YEBS + RGS for 2 days, alongside a mitochondrial-targeted red fluorescent protein IVD-FP611 (in pZP212). Following the protocol previously described (Mangano, Gonzalez and Petruccelli, 2014), ~4 week old *N. benthiamiana* leaves were syringe infiltrated on the abaxial surface with bacterial preparations (OD = 0.35 of each line). Plants were left to recover in a growth chamber for 48 hours before imaging.

Stable transformation of *A. thaliana*

~4 week old Col-0 and mito-mCherry plants were transformed via floral dip with *Agrobacterium* carrying either AOX or IVD-mt-Kaede-HINESS-HA constructs. A previously published protocol was followed (Zhang *et al.*, 2006), using a 5% (wt/vol) sucrose solution at pH 5.6 to resuspend cultured bacteria, and a second dip was performed 7 days after the first. Seeds were left to develop before screening with BASTA on soil.

BASTA® treatment for transformed Arabidopsis screening

Glufosinate Ammonium (BASTA®, plantmedia.com) was diluted to 300µM in a spray bottle with ddH_2O and sprayed upon seeds before stratification, then also to newly emerged seedlings and 1-2 week old plants, removed from growth chambers. Col-0 (susceptible) and pUBdest transformed (resistant) plants were grown alongside to monitor the effectiveness of treatment. Once sprayed, trays were left with plastic domed lids on for 8 hours before returning to the growth chamber.

Root and rosette assays

Seeds of each genotype were bleach sterilised and sown onto square plates (9x9cm), after stratification at 4˚C for 2 days, placed at a 70˚ angle in a growth cabinet and grown for 9 days without disturbance. Images were taken using the brightfield setting on a GelDoc Imager. Root lengths were hand traced from cotyledon base to root tip with the flexible line tool in ImageJ, after setting the scale based on the plate size, lengths were exported and further analysed in R.

For rosettes, seeds were grown on upright plates for 11 days before sowing on soil and growing for another 19 days. Rosette images were traced using freehand draw in ImageJ and the area was taken after setting the scale for pot size, exported and analysed in R.

Immunodetection of mitochondrial proteins

For each line, 50mg of 23-day-old seedlings were frozen in dry ice (kindly provided by Jithesh Vijayan), ground in 2mL cold homogenisation buffer (40mM HEPES, 0.4M D-sorbitol, 2mM EDTA, 50µM PVP40, 14.4mM ß-mercaptoethanol), passed once through Miracloth, and once through a 100µm filter to extract the total homogenate, centrifuged at 17,200g for 30mins at 4˚C, resuspending each in 30µL 1X Laemmli Buffer (BioRad #1610747).

Standard immunodetection techniques were followed using 10µL of each sample loaded into miniprotean TGX stain-free gels (BioRad #4568094), using dilute loading buffer (BioRad #1610732), and Precision Plus marker (BioRad #1610374), and run at 200V until separation, and imaged via GelDoc Go.

Following migration, proteins were transferred onto a nitrocellulose membrane (BioRad, #1620213), using the BioRad trans-blot (#1704150), blocked in EveryBlot Buffer (BioRad, #12010020) and incubated in primary antibodies from Agrisera AB (Sweden): CoxII at 1:1000 (#AS04053A), AtpB at 1:1000 (#AS163976), PsbA at 1:10,000 (#AS05084) and H3 at 1:5000 (#AS10710), then goat anti-rabbit secondary antibody from Southern Biotech (USA) (#4050-04). Final color detection was via the AP conjugate substrate kit (BioRad #1706432), and imaged via GelDoc Go.

<u>Oxygen consumption measurements</u>

~60 (±1) mg of leaf discs (7mm width) were cut from the middle tip region of 25-day-old *Arabidopsis* leaves and placed in respiratory activity incubation medium (10mM HEPES, 10mM MES, 2mM $CaCl_2$, pH 7.2) for 30 mins in the dark. Oxygen consumption measurements were taken using the Oxygraph+ oxygen electrode system (Hansatech Instruments, Pentney, Norfolk, UK), following (Sew et al., 2013). Calibration by removal of all oxygen in 1mL ddH_2O was performed using an excess of Sodium dithionate. Oxygen concentration was read over 15mins in the dark in 2mL of respiratory activity incubation medium, and oxygen consumption rate was calculated as nmol O_2 per minute per gram of fresh weight (FW).

Acknowledgements

We thank Prof. You (Joe) Zhou and Dr. Bara Altartouri of the Microscopy Core at the Nebraska Centre for Biotechnology for their invaluable help and microscopy advice. Thank you to Dr. Heather Jensen-Smith at the University of Nebraska Medical Centre Advanced Microscopy Core for access and advice on the IMARIS software. Thanks to Prof. Timothy Shutt (University of Calgary) and his team for the kind gift of the mt-HI-NESS construct. We thank Dr. Huang Li and Prof. Jeff Mower (University of Nebraska-Lincoln) for the use of the Hansatech Oxygraph+ system. We thank Prof. Christian Elowsky for his imaging advice and encouragement, and Dr. Kostas Giannakis for fruitful conversations on network analysis. Also, to Ana Martinez-Hottovy and Moira Rodriguez for their critical reading of the manuscript. This work was funded in part by a grant from the National Science Foundation to ACC (MCB-1933590). Major support was from a University of Nebraska Foundation fund in memory of Frank and Edith Christensen.

Author contributions

JMC and ACC designed the research. AQS and MHF conducted experiments. JMC conducted experiments, performed imaging, image analysis and data analysis. JMC and ACC wrote the manuscript. All authors edited the manuscript.

References

Alam, T. I., Kanki, T., Muta, T., Ukaji, K., Abe, Y., Nakayama, H., Takio, K., Hamasaki, N., & Kang, D. (2003). Human mitochondrial DNA is packaged with TFAM. *Nucleic Acids Research*, *31*(6), 1640–1645. https://doi.org/10.1093/nar/gkg251

Arimura, S. I. (2018). Fission and fusion of plant mitochondria, and genome maintenance. *Plant Physiology*, *176*(1), 152–161. https://doi.org/10.1104/pp.17.01025

Arimura, S. -i., Yamamoto, J., Aida, G. P., Nakazono, M., & Tsutsumi, N. (2004).

Frequent fusion and fission of plant mitochondria with unequal nucleoid distribution. *Proceedings of the National Academy of Sciences*, *101*(20), 7805–7808. https://doi.org/10.1073/pnas.0401077101

Avisar, D., Abu-Abied, M., Belausov, E., Sadot, E., Hawes, C., & Sparkes, I. A. (2009). A comparative study of the involvement of 17 Arabidopsis myosin family members on the motility of Golgi and other organelles. *Plant Physiology*, *150*(2), 700–709. https://doi.org/10.1104/pp.109.136853

Avisar, D., Prokhnevsky, A. I., Makarova, K. S., Koonin, E. V., & Dolja, V. V. (2008). Myosin XI-K Is Required for Rapid Trafficking of Golgi Stacks, Peroxisomes, and Mitochondria in Leaf Cells of Nicotiana benthamiana. *Plant Physiology*, *146*(3), 1098–1108. https://doi.org/10.1104/pp.107.113647

Baudier, J. (2018). ATAD3 proteins: Brokers of a mitochondria–endoplasmic reticulum connection in mammalian cells. *Biological Reviews*, *93*(2), 827–844. https://doi.org/10.1111/brv.12373

Bauwe, H., Hagemann, M., & Fernie, A. R. (2010). Photorespiration: Players, partners and origin. *Trends in Plant Science*, *15*(6), 330–336. https://doi.org/10.1016/j.tplants.2010.03.006

Candat, A., Paszkiewicz, G., Neveu, M., Gautier, R., Logan, D. C., Avelange-Macherel, M.-H., & Macherel, D. (2014). The Ubiquitous Distribution of Late Embryogenesis Abundant Proteins across Cell Compartments in Arabidopsis Offers Tailored Protection against Abiotic Stress. *The Plant Cell*, *26*(7), 3148–3166. https://doi.org/10.1105/tpc.114.127316

Christensen, A. C. (2014). Genes and junk in plant mitochondria-repair mechanisms and selection. *Genome Biology and Evolution*, *6*(6), 1448–1453. https://doi.org/10.1093/gbe/evu115

Chustecki, J. M., Etherington, R. D., Gibbs, D. J., & Johnston, I. G. (2021). Altered collective mitochondrial dynamics in an Arabidopsis msh1 mutant compromising organelle DNA maintenance. *bioRxiv*, 2021.10.22.465420. https://doi.org/10.1101/2021.10.22.465420

Chustecki, J. M., Etherington, R. D., Gibbs, D. J., & Johnston, I. G. (2022). Altered collective mitochondrial dynamics in the Arabidopsis msh1 mutant compromising

organelle DNA maintenance. *Journal of Experimental Botany*, *73*(16), 5428–5439. https://doi.org/10.1093/jxb/erac250

Chustecki, J. M., Gibbs, D. J., Bassel, G. W., & Johnston, I. G. (2021). Network analysis of Arabidopsis mitochondrial dynamics reveals a resolved tradeoff between physical distribution and social connectivity. *Cell Systems*, *12*(0), 1–13. https://doi.org/10.1016/j.cels.2021.04.006

Deng, J., Swift, L., Shahhosseini, F., Jaiswal, A., Brideau, C., Colarusso, P., & Shutt, T. E. (2023). A novel genetic fluorescent reporter to visualize mitochondrial nucleoids. *bioRxiv*, 2023–10.

Fuchs, P., Rugen, N., Carrie, C., Elsässer, M., Finkemeier, I., Giese, J., Hildebrandt, T. M., Kühn, K., Maurino, V. G., Ruberti, C., Schallenberg-Rüdinger, M., Steinbeck, J., Braun, H. P., Eubel, H., Meyer, E. H., Müller-Schüssele, S. J., & Schwarzländer, M. (2020). Single organelle function and organization as estimated from Arabidopsis mitochondrial proteomics. *The Plant Journal*, *101*(2), 420–441. https://doi.org/10.1111/TPJ.14534

Fuchs, R., Kopischke, M., Klapprodt, C., Hause, G., Meyer, A. J., Schwarzländer, M., Fricker, M. D., & Lipka, V. (2016). Immobilized Subpopulations of Leaf Epidermal Mitochondria Mediate PENETRATION2-Dependent Pathogen Entry Control in Arabidopsis. *The Plant Cell*, *28*(1), 130–145. https://doi.org/10.1105/tpc.15.00887

Giannakis, K., Chustecki, J. M., & Johnston, I. G. (2022). Exchange on dynamic encounter networks allows plant mitochondria to collect complete sets of mitochondrial DNA products despite their incomplete genomes. *Quantitative Plant Biology*, *3*, e18. https://doi.org/10.1017/qpb.2022.15

Green, M. R., & Sambrook, J. (2012). *Molecular Cloning: A Laboratory Manual*. Cold Spring Harbor Laboratory Press.

Gualberto, J. M., Mileshina, D., Wallet, C., Niazi, A. K., Weber-Lotfi, F., & Dietrich, A. (2014). The plant mitochondrial genome: Dynamics and maintenance. In *Biochimie* (Vol. 100, Issue 1, pp. 107–120). Elsevier. https://doi.org/10.1016/j.biochi.2013.09.016

Hagemann, M., Weber, A. P., & Eisenhut, M. (2016). Photorespiration: Origins and metabolic integration in interacting compartments. *Journal of Experimental*

Botany, *67*(10), 2915–2918. https://doi.org/10.1093/jxb/erw178

Hänselmann, S., & Herten, D.-P. (2017). Two-Color Single-Molecule Tracking in Live Cells. In H. Erfle (Ed.), *Super-Resolution Microscopy: Methods and Protocols* (pp. 127–138). Springer. https://doi.org/10.1007/978-1-4939-7265-4_11

Herlan, M., Bornhövd, C., Hell, K., Neupert, W., & Reichert, A. S. (2004). Alternative topogenesis of Mgm1 and mitochondrial morphology depend on ATP and a functional import motor. *Journal of Cell Biology*, *165*(2), 167–173. https://doi.org/10.1083/jcb.200403022

Johnston, I. G. (2019). Tension and Resolution: Dynamic, Evolving Populations of Organelle Genomes within Plant Cells. *Molecular Plant*, *12*(6), 764–783. https://doi.org/10.1016/j.molp.2018.11.002

Kim, M., Schulz, V., Brings, L., Schoeller, T., Kühn, K., & Vierling, E. (2021). mTERF18 and ATAD3 are required for mitochondrial nucleoid structure and their disruption confers heat tolerance in Arabidopsis thaliana. *New Phytologist*, *232*(5), 2026–2042. https://doi.org/10.1111/nph.17717

Kozik, A., Rowan, B. A., Lavelle, D., Berke, L., Eric Schranz, M., Michelmore, R. W., & Christensen, A. C. (2019). The alternative reality of plant mitochondrial DNA: One ring does not rule them all. *PLoS Genetics*, *15*(8). https://doi.org/10.1371/JOURNAL.PGEN.1008373

Kukat, C., Wurm, C. A., Spåhr, H., Falkenberg, M., Larsson, N. G., & Jakobs, S. (2011). Super-resolution microscopy reveals that mammalian mitochondrial nucleoids have a uniform size and frequently contain a single copy of mtDNA. *Proceedings of the National Academy of Sciences of the United States of America*, *108*(33), 13534–13539. https://doi.org/10.1073/PNAS.1109263108/-/DCSUPPLEMENTAL

Kumar, R. A., Oldenburg, D. J., & Bendich, A. J. (2014). Changes in DNA damage, molecular integrity, and copy number for plastid DNA and mitochondrial DNA during maize development. *Journal of Experimental Botany*, *65*(22), 6425–6439. https://doi.org/10.1093/jxb/eru359

Kuznetsov, A. V., & Margreiter, R. (2009). Heterogeneity of Mitochondria and Mitochondrial Function within Cells as Another Level of Mitochondrial Complexity. *International Journal of Molecular Sciences*, *10*(4), 1911–1929.

https://doi.org/10.3390/ijms10041911

Kuznetsov, A. V., Troppmair, J., Sucher, R., Hermann, M., Saks, V., & Margreiter, R. (2006). Mitochondrial subpopulations and heterogeneity revealed by confocal imaging: Possible physiological role? *Biochimica et Biophysica Acta (BBA) - Bioenergetics*, *1757*(5–6), 686–691. https://doi.org/10.1016/J.BBABIO.2006.03.014

Logan, D. C. (2006). The mitochondrial compartment. *Journal of Experimental Botany*, *57*(6), 1225–1243.

Michelson, A. A. (1995). *Studies in optics*. Courier Corporation.

Midorikawa, K., Tateishi, A., Toyooka, K., Sato, M., Imai, T., Kodama, Y., & Numata, K. (2022). Three-dimensional nanoscale analysis of light-dependent organelle changes in Arabidopsis mesophyll cells. *PNAS Nexus*, *1*(5), pgac225. https://doi.org/10.1093/pnasnexus/pgac225

Mueller, S. J., & Reski, R. (2015). Mitochondrial dynamics and the ER: The plant perspective. *Frontiers in Cell and Developmental Biology*, *3*(DEC), 78. https://doi.org/10.3389/fcell.2015.00078

Oldenburg, D. J., & Bendich, A. J. (2015). DNA maintenance in plastids and mitochondria of plants. *Frontiers in Plant Science*, *6*. https://doi.org/10.3389/fpls.2015.00883

Peremyslov, V. V., Cole, R. A., Fowler, J. E., & Dolja, V. V. (2015). Myosin-Powered Membrane Compartment Drives Cytoplasmic Streaming, Cell Expansion and Plant Development. *PLOS ONE*, *10*(10), e0139331. https://doi.org/10.1371/journal.pone.0139331

Preuten, T., Cincu, E., Fuchs, J., Zoschke, R., Liere, K., & Börner, T. (2010). Fewer genes than organelles: Extremely low and variable gene copy numbers in mitochondria of somatic plant cells. *The Plant Journal*, *64*(6), 948–959. https://doi.org/10.1111/j.1365-313X.2010.04389.x

Prole, D. L., Chinnery, P. F., & Jones, N. S. (2020). Visualizing, quantifying, and manipulating mitochondrial DNA in vivo. *The Journal of Biological Chemistry*, *295*(51), 17588. https://doi.org/10.1074/JBC.REV120.015101

Qiang, Y., Lee, J. Y., Bartenschlager, R., & Rohr, K. (2017). Colocalization analysis and

particle tracking in multi-channel fluorescence microscopy images. *2017 IEEE 14th International Symposium on Biomedical Imaging (ISBI 2017)*, 646–649. https://doi.org/10.1109/ISBI.2017.7950603

Rey, T., Tábara, L. C., Prudent, J., & Minczuk, M. (2023). mtFociCounter for automated single-cell mitochondrial nucleoid quantification and reproducible foci analysis. *Nucleic Acids Research*, *51*(21), e107–e107.

Rodriguez, M., Martinez-Hottovy, A., & Christensen, A. C. (2022). Social networks in the single cell. *Journal of Experimental Botany*, *73*(16), 5355–5357. https://doi.org/10.1093/JXB/ERAC284

Romagnoli, S., Cai, G., Faleri, C., Yokota, E., Shimmen, T., & Cresti, M. (2007). Microtubule- and Actin Filament-Dependent Motors are Distributed on Pollen Tube Mitochondria and Contribute Differently to Their Movement. *Plant and Cell Physiology*, *48*(2), 345–361. https://doi.org/10.1093/pcp/pcm001

Sew, Y. S., Ströher, E., Holzmann, C., Huang, S., Taylor, N. L., Jordana, X., & Millar, A. H. (2013). Multiplex micro-respiratory measurements of Arabidopsis tissues. *New Phytologist*, *200*(3), 922–932. https://doi.org/10.1111/nph.12394

Sheahan, M. B., McCurdy, D. W., & Rose, R. J. (2005). Mitochondria as a connected population: Ensuring continuity of the mitochondrial genome during plant cell dedifferentiation through massive mitochondrial fusion. *Plant Journal*, *44*(5), 744–755. https://doi.org/10.1111/j.1365-313X.2005.02561.x

Shimmen, T., & Yokota, E. (2004). Cytoplasmic streaming in plants. *Current Opinion in Cell Biology*, *16*(1), 68–72. https://doi.org/10.1016/j.ceb.2003.11.009

Sparkes, I. A., Teanby, N. A., & Hawes, C. (2008). Truncated myosin XI tail fusions inhibit peroxisome, Golgi, and mitochondrial movement in tobacco leaf epidermal cells: A genetic tool for the next generation. *Journal of Experimental Botany*, *59*(9), 2499–2512. https://doi.org/10.1093/jxb/ern114

Spilger, R., Lee, J.-Y., Bartenschlager, R., & Rohr, K. (2022). Deep Neural Network for Combined Particle Tracking and Colocalization Analysis in Two-Channel Microscopy Images. *2022 IEEE 19th International Symposium on Biomedical Imaging (ISBI)*, 1–4. https://doi.org/10.1109/ISBI52829.2022.9761696

Stephen J Royle. (2024). *TrackMateR: Working with TrackMate outputs in R*.

https://quantixed.github.io/TrackMateR/

Takanashi, H., Arimura, S. I., Sakamoto, W., & Tsutsumi, N. (2006). Different amounts of DNA in each mitochondrion in rice root. *Genes and Genetic Systems*, *81*(3), 215–218. https://doi.org/10.1266/ggs.81.215

Tinevez, J. Y., Perry, N., Schindelin, J., Hoopes, G. M., Reynolds, G. D., Laplantine, E., Bednarek, S. Y., Shorte, S. L., & Eliceiri, K. W. (2017). TrackMate: An open and extensible platform for single-particle tracking. *Methods*, *115*, 80–90. https://doi.org/10.1016/j.ymeth.2016.09.016

Tominaga, M., & Ito, K. (2015). The molecular mechanism and physiological role of cytoplasmic streaming. *Current Opinion in Plant Biology*, *27*, 104–110. https://doi.org/10.1016/j.pbi.2015.06.017

Tominaga, M., Kojima, H., Yokota, E., Orii, H., Nakamori, R., Katayama, E., Anson, M., Shimmen, T., & Oiwa, K. (2003). Higher plant myosin XI moves processively on actin with 35 nm steps at high velocity. *The EMBO Journal*, *22*(6), 1263–1272. https://doi.org/10.1093/emboj/cdg130

Twig, G., Elorza, A., Molina, A. J. A., Mohamed, H., Wikstrom, J. D., Walzer, G., Stiles, L., Haigh, S. E., Katz, S., Las, G., Alroy, J., Wu, M., Py, B. F., Yuan, J., Deeney, J. T., Corkey, B. E., & Shirihai, O. S. (2008). Fission and selective fusion govern mitochondrial segregation and elimination by autophagy. *The EMBO Journal*, *27*(2), 433–446. https://doi.org/10.1038/sj.emboj.7601963

Wagner, T. (2016). *ij-trackmate-findmaxima: FindMaxima-1.0.1* (Version FindMaxima-1.0.1) [Computer software]. Zenodo. https://doi.org/10.5281/zenodo.59166

White, R. R., Lin, C., Leaves, I., Castro, I. G., Metz, J., Bateman, B. C., Botchway, S. W., Ward, A. D., Ashwin, P., & Sparkes, I. (2020). Miro2 tethers the ER to mitochondria to promote mitochondrial fusion in tobacco leaf epidermal cells. *Communications Biology*, *3*(1), 1–8. https://doi.org/10.1038/s42003-020-0872-x

Willingham, T. B., Ajayi, P. T., & Glancy, B. (2021). Subcellular Specialization of Mitochondrial Form and Function in Skeletal Muscle Cells. *Frontiers in Cell and Developmental Biology*, *9*, 2907. https://doi.org/10.3389/FCELL.2021.757305/BIBTEX

Zheng, M., Wang, Q., Teng, Y., Wang, X., Wang, F., Chen, T., Šamaj, J., Lin, J., &

Logan, D. C. (2010). The speed of mitochondrial movement is regulated by the cytoskeleton and myosin in Picea wilsonii pollen tubes. *Planta*, *231*(4), 779–791. https://doi.org/10.1007/s00425-009-1086-0

Parsed Citations

Alam, T. I., Kanki, T., Muta, T., Ukaji, K., Abe, Y., Nakayama, H., Takio, K., Hamasaki, N., & Kang, D. (2003). Human mitochondrial DNA is packaged with TFAM. Nucleic Acids Research, 31(6), 1640–1645. https://doi.org/10.1093/nar/gkg251
Google Scholar: Author Only Title Only Author and Title

Arimura, S. I. (2018). Fission and fusion of plant mitochondria, and genome maintenance. Plant Physiology, 176(1), 152–161. https://doi.org/10.1104/pp.17.01025
Google Scholar: Author Only Title Only Author and Title

Arimura, S. -i., Yamamoto, J., Aida, G. P., Nakazono, M., & Tsutsumi, N. (2004). Frequent fusion and fission of plant mitochondria with unequal nucleoid distribution. Proceedings of the National Academy of Sciences, 101(20), 7805–7808. https://doi.org/10.1073/pnas.0401077101
Google Scholar: Author Only Title Only Author and Title

Avisar, D., Abu-Abied, M., Belausov, E., Sadot, E., Hawes, C., & Sparkes, I. A. (2009). A comparative study of the involvement of 17 Arabidopsis myosin family members on the motility of Golgi and other organelles. Plant Physiology, 150(2), 700–709. https://doi.org/10.1104/pp.109.136853
Google Scholar: Author Only Title Only Author and Title

Avisar, D., Prokhnevsky, A. I., Makarova, K. S., Koonin, E. V., & Dolja, V. V. (2008). Myosin XI-K Is Required for Rapid Trafficking of Golgi Stacks, Peroxisomes, and Mitochondria in Leaf Cells of Nicotiana benthamiana. Plant Physiology, 146(3), 1098–1108. https://doi.org/10.1104/pp.107.113647
Google Scholar: Author Only Title Only Author and Title

Baudier, J. (2018). ATAD3 proteins: Brokers of a mitochondria–endoplasmic reticulum connection in mammalian cells. Biological Reviews, 93(2), 827–844. https://doi.org/10.1111/brv.12373
Google Scholar: Author Only Title Only Author and Title

Bauwe, H., Hagemann, M., & Fernie, A. R. (2010). Photorespiration: Players, partners and origin. Trends in Plant Science, 15(6), 330–336. https://doi.org/10.1016/j.tplants.2010.03.006
Google Scholar: Author Only Title Only Author and Title

Candat, A., Paszkiewicz, G., Neveu, M., Gautier, R., Logan, D. C., Avelange-Macherel, M.-H., & Macherel, D. (2014). The Ubiquitous Distribution of Late Embryogenesis Abundant Proteins across Cell Compartments in Arabidopsis Offers Tailored Protection against Abiotic Stress. The Plant Cell, 26(7), 3148–3166. https://doi.org/10.1105/tpc.114.127316
Google Scholar: Author Only Title Only Author and Title

Christensen, A. C. (2014). Genes and junk in plant mitochondria-repair mechanisms and selection. Genome Biology and Evolution, 6(6), 1448–1453. https://doi.org/10.1093/gbe/evu115
Google Scholar: Author Only Title Only Author and Title

Chustecki, J. M., Etherington, R. D., Gibbs, D. J., & Johnston, I. G. (2021). Altered collective mitochondrial dynamics in an Arabidopsis msh1 mutant compromising organelle DNA maintenance. bioRxiv, 2021.10.22.465420. https://doi.org/10.1101/2021.10.22.465420
Google Scholar: Author Only Title Only Author and Title

Chustecki, J. M., Etherington, R. D., Gibbs, D. J., & Johnston, I. G. (2022). Altered collective mitochondrial dynamics in the Arabidopsis msh1 mutant compromising organelle DNA maintenance. Journal of Experimental Botany, 73(16), 5428–5439. https://doi.org/10.1093/jxb/erac250
Google Scholar: Author Only Title Only Author and Title

Chustecki, J. M., Gibbs, D. J., Bassel, G. W., & Johnston, I. G. (2021). Network analysis of Arabidopsis mitochondrial dynamics reveals a resolved tradeoff between physical distribution and social connectivity. Cell Systems, 12(0), 1–13. https://doi.org/10.1016/j.cels.2021.04.006
Google Scholar: Author Only Title Only Author and Title

Deng, J., Swift, L., Shahhosseini, F., Jaiswal, A., Brideau, C., Colarusso, P., & Shutt, T. E. (2023). A novel genetic fluorescent reporter to visualize mitochondrial nucleoids. bioRxiv, 2023–10.
Google Scholar: Author Only Title Only Author and Title

Fuchs, P., Rugen, N., Carrie, C., Elsässer, M., Finkemeier, I., Giese, J., Hildebrandt, T. M., Kühn, K., Maurino, V. G., Ruberti, C., Schallenberg-Rüdinger, M., Steinbeck, J., Braun, H. P., Eubel, H., Meyer, E. H., Müller-Schüssele, S. J., & Schwarzländer, M. (2020). Single organelle function and organization as estimated from Arabidopsis mitochondrial proteomics. The Plant Journal, 101(2), 420–441. https://doi.org/10.1111/TPJ.14534
Google Scholar: Author Only Title Only Author and Title

Fuchs, R., Kopischke, M., Klapprodt, C., Hause, G., Meyer, A. J., Schwarzländer, M., Fricker, M. D., & Lipka, V. (2016). Immobilized Subpopulations of Leaf Epidermal Mitochondria Mediate PENETRATION2-Dependent Pathogen Entry Control in Arabidopsis. The Plant Cell, 28(1), 130–145. https://doi.org/10.1105/tpc.15.00887

Google Scholar: Author Only Title Only Author and Title

Giannakis, K., Chustecki, J. M., & Johnston, I. G. (2022). Exchange on dynamic encounter networks allows plant mitochondria to collect complete sets of mitochondrial DNA products despite their incomplete genomes. Quantitative Plant Biology, 3, e18. https://doi.org/10.1017/qpb.2022.15
Google Scholar: Author Only Title Only Author and Title

Green, M. R., & Sambrook, J. (2012). Molecular Cloning: A Laboratory Manual. Cold Spring Harbor Laboratory Press.
Google Scholar: Author Only Title Only Author and Title

Gualberto, J. M., Mileshina, D., Wallet, C., Niazi, A. K., Weber-Lotfi, F., & Dietrich, A. (2014). The plant mitochondrial genome: Dynamics and maintenance. In Biochimie (Vol. 100, Issue 1, pp. 107–120). Elsevier. https://doi.org/10.1016/j.biochi.2013.09.016
Google Scholar: Author Only Title Only Author and Title

Hagemann, M., Weber, A. P., & Eisenhut, M. (2016). Photorespiration: Origins and metabolic integration in interacting compartments. Journal of Experimental Botany, 67(10), 2915–2918. https://doi.org/10.1093/jxb/erw178
Google Scholar: Author Only Title Only Author and Title

Hänselmann, S., & Herten, D.-P. (2017). Two-Color Single-Molecule Tracking in Live Cells. In H. Erfle (Ed.), Super-Resolution Microscopy: Methods and Protocols (pp. 127–138). Springer. https://doi.org/10.1007/978-1-4939-7265-4_11
Google Scholar: Author Only Author and Title

Herlan, M., Bornhövd, C., Hell, K., Neupert, W., & Reichert, A. S. (2004). Alternative topogenesis of Mgm1 and mitochondrial morphology depend on ATP and a functional import motor. Journal of Cell Biology, 165(2), 167–173. https://doi.org/10.1083/jcb.200403022
Google Scholar: Author Only Title Only Author and Title

Johnston, I. G. (2019). Tension and Resolution: Dynamic, Evolving Populations of Organelle Genomes within Plant Cells. Molecular Plant, 12(6), 764–783. https://doi.org/10.1016/j.molp.2018.11.002
Google Scholar: Author Only Title Only Author and Title

Kim, M., Schulz, V., Brings, L., Schoeller, T., Kühn, K., & Vierling, E. (2021). mTERF18 and ATAD3 are required for mitochondrial nucleoid structure and their disruption confers heat tolerance in Arabidopsis thaliana. New Phytologist, 232(5), 2026–2042. https://doi.org/10.1111/nph.17717
Google Scholar: Author Only Title Only Author and Title

Kozik, A., Rowan, B. A., Lavelle, D., Berke, L., Eric Schranz, M., Michelmore, R. W., & Christensen, A. C. (2019). The alternative reality of plant mitochondrial DNA: One ring does not rule them all. PLoS Genetics, 15(8). https://doi.org/10.1371/JOURNAL.PGEN.1008373
Google Scholar: Author Only Title Only Author and Title

Kukat, C., Wurm, C. A., Spåhr, H., Falkenberg, M., Larsson, N. G., & Jakobs, S. (2011). Super-resolution microscopy reveals that mammalian mitochondrial nucleoids have a uniform size and frequently contain a single copy of mtDNA. Proceedings of the National Academy of Sciences of the United States of America, 108(33), 13534–13539. https://doi.org/10.1073/PNAS.1109263108/-/DCSUPPLEMENTAL
Google Scholar: Author Only Title Only Author and Title

Kumar, R. A., Oldenburg, D. J., & Bendich, A. J. (2014). Changes in DNA damage, molecular integrity, and copy number for plastid DNA and mitochondrial DNA during maize development. Journal of Experimental Botany, 65(22), 6425–6439. https://doi.org/10.1093/jxb/eru359
Google Scholar: Author Only Title Only Author and Title

Kuznetsov, A. V., & Margreiter, R. (2009). Heterogeneity of Mitochondria and Mitochondrial Function within Cells as Another Level of Mitochondrial Complexity. International Journal of Molecular Sciences, 10(4), 1911–1929. https://doi.org/10.3390/ijms10041911
Google Scholar: Author Only Title Only Author and Title

Kuznetsov, A. V., Troppmair, J., Sucher, R., Hermann, M., Saks, V., & Margreiter, R. (2006). Mitochondrial subpopulations and heterogeneity revealed by confocal imaging: Possible physiological role? Biochimica et Biophysica Acta (BBA) - Bioenergetics, 1757(5–6), 686–691. https://doi.org/10.1016/J.BBABIO.2006.03.014
Google Scholar: Author Only Title Only Author and Title

Logan, D. C. (2006). The mitochondrial compartment. Journal of Experimental Botany, 57(6), 1225–1243.
Google Scholar: Author Only Title Only Author and Title

Michelson, A. A. (1995). Studies in optics. Courier Corporation.
Google Scholar: Author Only Title Only Author and Title

Midorikawa, K., Tateishi, A., Toyooka, K., Sato, M., Imai, T., Kodama, Y., & Numata, K. (2022). Three-dimensional nanoscale analysis of light-dependent organelle changes in Arabidopsis mesophyll cells. PNAS Nexus, 1(5), pgac225.

https://doi.org/10.1093/pnasnexus/pgac225
Google Scholar: Author Only Title Only Author and Title

Mueller, S. J., & Reski, R. (2015). Mitochondrial dynamics and the ER: The plant perspective. Frontiers in Cell and Developmental Biology, 3(DEC), 78. https://doi.org/10.3389/fcell.2015.00078
Google Scholar: Author Only Title Only Author and Title

Oldenburg, D. J., & Bendich, A. J. (2015). DNA maintenance in plastids and mitochondria of plants. Frontiers in Plant Science, 6. https://doi.org/10.3389/fpls.2015.00883
Google Scholar: Author Only Title Only Author and Title

Peremyslov, V. V., Cole, R. A., Fowler, J. E., & Dolja, V. V. (2015). Myosin-Powered Membrane Compartment Drives Cytoplasmic Streaming, Cell Expansion and Plant Development. PLOS ONE, 10(10), e0139331. https://doi.org/10.1371/journal.pone.0139331
Google Scholar: Author Only Title Only Author and Title

Preuten, T., Cincu, E., Fuchs, J., Zoschke, R., Liere, K., & Börner, T. (2010). Fewer genes than organelles: Extremely low and variable gene copy numbers in mitochondria of somatic plant cells. The Plant Journal, 64(6), 948–959. https://doi.org/10.1111/j.1365-313X.2010.04389.x
Google Scholar: Author Only Title Only Author and Title

Prole, D. L., Chinnery, P. F., & Jones, N. S. (2020). Visualizing, quantifying, and manipulating mitochondrial DNA in vivo. The Journal of Biological Chemistry, 295(51), 17588. https://doi.org/10.1074/JBC.REV120.015101
Google Scholar: Author Only Title Only Author and Title

Qiang, Y., Lee, J. Y., Bartenschlager, R., & Rohr, K. (2017). Colocalization analysis and particle tracking in multi-channel fluorescence microscopy images. 2017 IEEE 14th International Symposium on Biomedical Imaging (ISBI 2017), 646–649. https://doi.org/10.1109/ISBI.2017.7950603
Google Scholar: Author Only Title Only Author and Title

Rey, T., Tábara, L. C., Prudent, J., & Minczuk, M. (2023). mtFociCounter for automated single-cell mitochondrial nucleoid quantification and reproducible foci analysis. Nucleic Acids Research, 51(21), e107–e107.
Google Scholar: Author Only Title Only Author and Title

Rodriguez, M., Martinez-Hottovy, A., & Christensen, A. C. (2022). Social networks in the single cell. Journal of Experimental Botany, 73(16), 5355–5357. https://doi.org/10.1093/JXB/ERAC284
Google Scholar: Author Only Title Only Author and Title

Romagnoli, S., Cai, G., Faleri, C., Yokota, E., Shimmen, T., & Cresti, M. (2007). Microtubule- and Actin Filament-Dependent Motors are Distributed on Pollen Tube Mitochondria and Contribute Differently to Their Movement. Plant and Cell Physiology, 48(2), 345–361. https://doi.org/10.1093/pcp/pcm001
Google Scholar: Author Only Title Only Author and Title

Sew, Y. S., Ströher, E., Holzmann, C., Huang, S., Taylor, N. L., Jordana, X., & Millar, A. H. (2013). Multiplex micro-respiratory measurements of Arabidopsis tissues. New Phytologist, 200(3), 922–932. https://doi.org/10.1111/nph.12394
Google Scholar: Author Only Title Only Author and Title

Sheahan, M. B., McCurdy, D. W., & Rose, R. J. (2005). Mitochondria as a connected population: Ensuring continuity of the mitochondrial genome during plant cell dedifferentiation through massive mitochondrial fusion. Plant Journal, 44(5), 744–755. https://doi.org/10.1111/j.1365-313X.2005.02561.x
Google Scholar: Author Only Title Only Author and Title

Shimmen, T., & Yokota, E. (2004). Cytoplasmic streaming in plants. Current Opinion in Cell Biology, 16(1), 68–72. https://doi.org/10.1016/j.ceb.2003.11.009
Google Scholar: Author Only Title Only Author and Title

Sparkes, I. A., Teanby, N. A., & Hawes, C. (2008). Truncated myosin XI tail fusions inhibit peroxisome, Golgi, and mitochondrial movement in tobacco leaf epidermal cells: A genetic tool for the next generation. Journal of Experimental Botany, 59(9), 2499–2512. https://doi.org/10.1093/jxb/ern114
Google Scholar: Author Only Title Only Author and Title

Spilger, R., Lee, J.-Y., Bartenschlager, R., & Rohr, K. (2022). Deep Neural Network for Combined Particle Tracking and Colocalization Analysis in Two-Channel Microscopy Images. 2022 IEEE 19th International Symposium on Biomedical Imaging (ISBI), 1–4. https://doi.org/10.1109/ISBI52829.2022.9761696
Google Scholar: Author Only Title Only Author and Title

Stephen J Royle. (2024). TrackMateR: Working with TrackMate outputs in R. https://quantixed.github.io/TrackMateR/
Google Scholar: Author Only Title Only Author and Title

Takanashi, H., Arimura, S. I., Sakamoto, W., & Tsutsumi, N. (2006). Different amounts of DNA in each mitochondrion in rice root. Genes and Genetic Systems, 81(3), 215–218. https://doi.org/10.1266/ggs.81.215

Google Scholar: Author Only Title Only Author and Title

Tinevez, J. Y., Perry, N., Schindelin, J., Hoopes, G. M., Reynolds, G. D., Laplantine, E., Bednarek, S. Y., Shorte, S. L., & Eliceiri, K. W. (2017). TrackMate: An open and extensible platform for single-particle tracking. Methods, 115, 80–90. https://doi.org/10.1016/j.ymeth.2016.09.016
Google Scholar: Author Only Title Only Author and Title

Tominaga, M., & Ito, K. (2015). The molecular mechanism and physiological role of cytoplasmic streaming. Current Opinion in Plant Biology, 27, 104–110. https://doi.org/10.1016/j.pbi.2015.06.017
Google Scholar: Author Only Title Only Author and Title

Tominaga, M., Kojima, H., Yokota, E., Orii, H., Nakamori, R., Katayama, E., Anson, M., Shimmen, T., & Oiwa, K. (2003). Higher plant myosin XI moves processively on actin with 35 nm steps at high velocity. The EMBO Journal, 22(6), 1263–1272. https://doi.org/10.1093/emboj/cdg130
Google Scholar: Author Only Title Only Author and Title

Twig, G., Elorza, A., Molina, A. J. A., Mohamed, H., Wikstrom, J. D., Walzer, G., Stiles, L., Haigh, S. E., Katz, S., Las, G., Alroy, J., Wu, M., Py, B. F., Yuan, J., Deeney, J. T., Corkey, B. E., & Shirihai, O. S. (2008). Fission and selective fusion govern mitochondrial segregation and elimination by autophagy. The EMBO Journal, 27(2), 433–446. https://doi.org/10.1038/sj.emboj.7601963
Google Scholar: Author Only Title Only Author and Title

Wagner, T. (2016). ij-trackmate-findmaxima: FindMaxima-1.0.1 (Version FindMaxima-1.0.1) [Computer software]. Zenodo. https://doi.org/10.5281/zenodo.59166
Google Scholar: Author Only Title Only Author and Title

White, R. R., Lin, C., Leaves, I., Castro, I. G., Metz, J., Bateman, B. C., Botchway, S. W., Ward, A. D., Ashwin, P., & Sparkes, I. (2020). Miro2 tethers the ER to mitochondria to promote mitochondrial fusion in tobacco leaf epidermal cells. Communications Biology, 3(1), 1–8. https://doi.org/10.1038/s42003-020-0872-x
Google Scholar: Author Only Title Only Author and Title

Willingham, T. B., Ajayi, P. T., & Glancy, B. (2021). Subcellular Specialization of Mitochondrial Form and Function in Skeletal Muscle Cells. Frontiers in Cell and Developmental Biology, 9, 2907. https://doi.org/10.3389/FCELL.2021.757305/BIBTEX
Google Scholar: Author Only Title Only Author and Title

Zheng, M., Wang, Q., Teng, Y., Wang, X., Wang, F., Chen, T., Šamaj, J., Lin, J., & Logan, D. C. (2010). The speed of mitochondrial movement is regulated by the cytoskeleton and myosin in Picea wilsonii pollen tubes. Planta, 231(4), 779–791. https://doi.org/10.1007/s00425-009-1086-0
Google Scholar: Author Only Title Only Author and Title